FATIGUE- RATCHETING INTERACTION BEHAVIOR OF AISI 4340 STEEL

A thesis submitted in partial fulfillment of the

Requirements for the degree of

Master of Technology (By Research)

in

Metallurgical and Materials Engineering

by

K. Divya Bharathi

(Roll Number - 613MM3003)

Under the supervision of

Prof. Krishna Dutta

Department of Metallurgical and Materials Engineering

National Institute of Technology Rourkela, Odisha

2015

Contents

National Institute of Technology
Rourkela

C E R T I F I C A T E

This is to certify that the thesis entitled ***Fatigue-Ratcheting Interaction Behavior of AISI 4340 Steel*** submitted by **K. DIVYA BHARATHI** to National Institute of Technology, Rourkela for the award of the degree of **Master of Technology (By Research)** in *Metallurgical and Materials Engineering* is an authentic record of research work carried out by her under my supervision.

The work incorporated in this thesis has not been, to the best of my knowledge, submitted to any other University or Institute for the award of a degree or diploma.

Date:
Place: Rourkela

Prof. Krishna Dutta
Assistant Professor
Department of Metallurgical and Materials Engineering,
National Institute of Technology, Rourkela

Acknowledgements

A journey is easier when you travel together. This thesis is the results of years of work whereby I have been guided and supported by many people. Hence, this would be worthwhile and pleasing to express sense of gratitude for all of them.

I would like to express my deep sense of gratitude to my supervisor **Prof. Krishna Dutta**, Assistant Professor, NIT, Rourkela for their invaluable guidance, motivation, untiring efforts, meticulous attention and support throughout my research work. It would have not been possible for me to bring out this thesis without his help and constant encouragement.

I am sincerely thankful to **Dr S.C. Mishra**, Professor and Head Metallurgical and Materials Engineering Department and other faculty members of this department for their persistent support and advice during the course work.

I am also highly grateful to laboratory members of Department of Metallurgical and Materials Engineering, NIT Rourkela, specially Mr. Hembram, Mr. R. Pattanaik, Mr. S. Pradhan and Mr. A. Pal for their help during the execution of experiment.

I wish to place my deep sense of thanks to my friends for their cooperation and critical suggestion during my project work and studies.

Finally, I feel great reverence for all my family members and the Almighty, for their blessings and for being a constant source of encouragement.

Date:

Place: **K. Divya Bharathi**

Abstract

Ratcheting is known as accumulation of plastic strain during asymmetric cyclic loading of materials under non-zero mean stress. This study intends to investigate the ratcheting behavior in AISI 4340 steel which is mainly used for designing of railway wheel sets, axles, shafts, aircraft components etc. The effect of stress ratio on the ratcheting behavior in both annealed and normalised conditions, effect of previous low cycle fatigue deformation on ratcheting behavior and vice versa were investigated for investigated steel. Ratcheting tests were done at different stress ratios of -0.4, -0.6 and -0.8 and strain controlled low cycle fatigue tests were done at strain amplitudes of ±0.50 and ±0.75. The results showed that cyclic hardening takes place during ratcheting deformation while strain accumulation increases with increasing stress ratio. Prior fatigue deformation induces more ratcheting strain in the material under same magnitudes of stress ratios. Post ratcheted samples showed increase in tensile strength and hardness which increases with increasing stress ratio and these variations in tensile properties are correlated with the induced cyclic hardening. The X-ray diffraction profile analysis using the modified Williamson–Hall equation has been carried out in order to estimate the dislocation densities in the specimens subjected to both ratcheting and low cycle fatigue. Increase in strain accumulation has been explained by increase in dislocation densities in the specimens and a correlation between the strain produced by ratcheting deformation and the estimated dislocation density has been established.

Keywords: Low cycle fatigue, Ratcheting, hardening behavior, optical microscopy, X-ray diffraction profile analysis, dislocation density.

List of Figures

List of Tables

CHAPTER 1

INTRODUCTION

INTRODUCTION

Since 1850, it was observed that machine components subjecting to cyclic loading, would fail at much lower stress levels than that required to cause failure under static loading. This type of failures was then named as “fatigue” and subsequently it was found that fatigue is an important deformation mechanism and almost about 90% of all engineering failures occur due to fatigue [1]. Since then enormous work has been carried out in order to study various aspects of fatigue failure and to develop different methods to prevent this phenomenon. The phenomenon of fatigue may be divided into several types depending upon cycles to failure; these are low cycle fatigue (LCF), high cycle fatigue (HCF), very low and very high cycle fatigue (VLCF and VHCF respectively) etc. Depending on the nature of accumulated strain, the fatigue behavior can be subdivided as ratcheting, mean stress or strain relaxation etc. Amongst these, damage accumulation by ratcheting is getting considerable attention in last two decades and now-a-days several research groups are studying ratcheting behavior of materials [2-10]. Ratcheting is a phenomenon of cyclic plasticity that can accelerate fatigue damage or even act as the failure mechanism itself [11]. It occurs during asymmetric cyclic loading, in presence of positive or negative mean stress and thus plastic strain gets accumulated during each cycle in the direction of the applied mean stress. Accumulation of ratcheting strain can substantially reduce the fatigue life of a component [12-17]. In practice, machine components can come across both ratcheting and fatigue simultaneously and therefore failure of a component can occur due to fatigue, ratcheting or due to combination of both the effects. So it will be a priori to understand combined effect of ratcheting and fatigue of a material before designing for a particular application to define its proper fatigue life and to avoid catastrophic failure.

Since few decades, enormous work has been reported on ratcheting behavior of various materials. Kang et al. [18, 19], Liu et al. [20] and Yoshida [21] focused on the interaction of fatigue and ratcheting of steel, and found the cyclic softening/hardening features affect the ratcheting behavior. Ray et al. [22], Dutta and Ray [23], Lee et al. [24], Lin et al. [25, 26] investigated ratcheting behavior of different steels and reported the

effect of stress amplitude and mean stress on ratcheting. Paul et al. [27], Wen et al. [28], Sarkar et al. [29], Pun et al. [30] and Yang [31] investigated ratcheting behavior of different steels and explained strain accumulation in prediction of ratcheting life. Kang et al. [32] and Cheng et al . [33] investigated the uniaxial time dependent ratcheting behavior of different steels at high temperature (300° C and 700° C) and they reported that ratcheting strain depends greatly on the stressing rate, holding time and ambient temperature. Chen and Hui [34], Tao and Xia [35, 36] and Shariati et al. [37] investigated the effects of loading rate, mean stress and stress amplitude on the ratcheting behavior of different polymers. The above investigations describe ratcheting behavior of different materials and only few of these reports represent combined effect of ratcheting behavior and LCF. But to refine our concepts on ratcheting and fatigue interactions, more experimental investigations are required to model the phenomena responsible for material behavior on presence of complex loadings.

Steels of various compositions play vital role in manufacturing of metal products and designing critical engineering structures from historical ages due to their high strength along with remarkable toughness. AISI 4340 steel is a kind of medium carbon steel which is traditionally used in aerospace applications (e.g. crank shafts and landing gears) and in automotive industries (e.g. connecting rods and axles); the steel is known to be subjected to normalising heat treatment before being designed to any component [38]. One cannot rule out the presence of ratcheting deformation during applications of such machine components. In mechanical designs, load conditions are presented by maximum stress and stress ratio, responding to maximum load and cyclic features. Hence maximum stress and stress ratio are chosen as control parameters for describing the stress features. Currently, only few reports exist on stress ratio effect and almost negligible amount of reports exist that focus ratcheting and fatigue interaction of such steel [39-41]. Hence it is of utmost importance to investigate the ratcheting behavior at different stress ratios and ratcheting fatigue interaction behavior of such steel. Therefore, in the present work, effect of stress ratio on ratcheting and the interaction of fatigue and ratcheting of AISI 4340 steel under differently heat treated (annealed and normalised) conditions has been studied. In view of these, the steel is subjected to fixed number ratcheting followed by LCF and vice versa.

Fractographic analysis after the fatigue test has been carried out using scanning electron microscope. Efforts have been made to correlate fractographic study of microstructure and fatigue strength at different heat treated conditions.

This thesis contains five chapters; Chapter 1 gives the information about importance of fatigue – ratcheting studies on the investigated AISI 4340 steel. Motivation and overview of present work is discussed in this chapter. Chapter 2 comprises of a review of previous investigations which are related to low cycle fatigue and ratcheting. Effect of strain amplitude, strain rate, stress amplitude etc. on LCF and effect of mean stress, stress amplitude on ratcheting are discussed. In published research papers the information gives the directions for further research and therefore, the present study is aimed to fulfill some gaps existing in previous investigations. Chapter 3 comprises the detailed information about the experiments which have been conducted in this work including heat treatment, hardness test, fatigue test, microstructural analysis, and grain size measurement. Chapter 4 comprises of results and discussion of hardness test, tensile test, fatigue test and microstructural analysis. The effect of grain size on combination of low cycle fatigue and ratcheting has been discussed. Variations of fracture surfaces of annealed and normalized steels after the fatigue test are also discussed. Chapter 5 presents the conclusions and summary of the present work. It also provides the directions for further investigation. At the end, the references followed during this investigation are enlisted.

CHAPTER 2

LITERATURE REVIEW

LITERATURE REVIEW

2.1 Fatigue of steel

Fatigue is a phenomenon that imposes small/high loads on materials repeatedly and leads to failure. These failures need to be avoided as they occur without any warning or indication [1]. Fatigue mainly occurs due to the following reasons:

1. A maximum tensile stress of sufficiently high value.
2. Large fluctuation in applied stress.
3. A very high cycle for the applied stress.

The various types of fluctuating loads that can lead to fatigue failure are given below:

Figure.2.1 (a) shows completely reversed cycle of stress. For this type of stress cycle the maximum and minimum stresses are equal but of opposite sign, In other words we can say symmetric loading ($\sigma_m = 0$). Tensile stress and compressive stress is considered positive and negative respectively. Figure 2.1 (b) shows repeated stress cycle where the maximum stress σ_{max} and σ_{min} are not equal [42, 43]. The figure shows that both σ_{max} and σ_{min} are in tension, but repeated stress cycle could contain maximum and minimum stresses of opposite sign or both in tension, which is known as asymmetric loading ($\sigma_m \neq 0$). A complicated stress cycle is shown in Fig. 2.1 (c), which might be encountered in an aircraft wing subjected to periodic unpredictable load due to gusts [39].

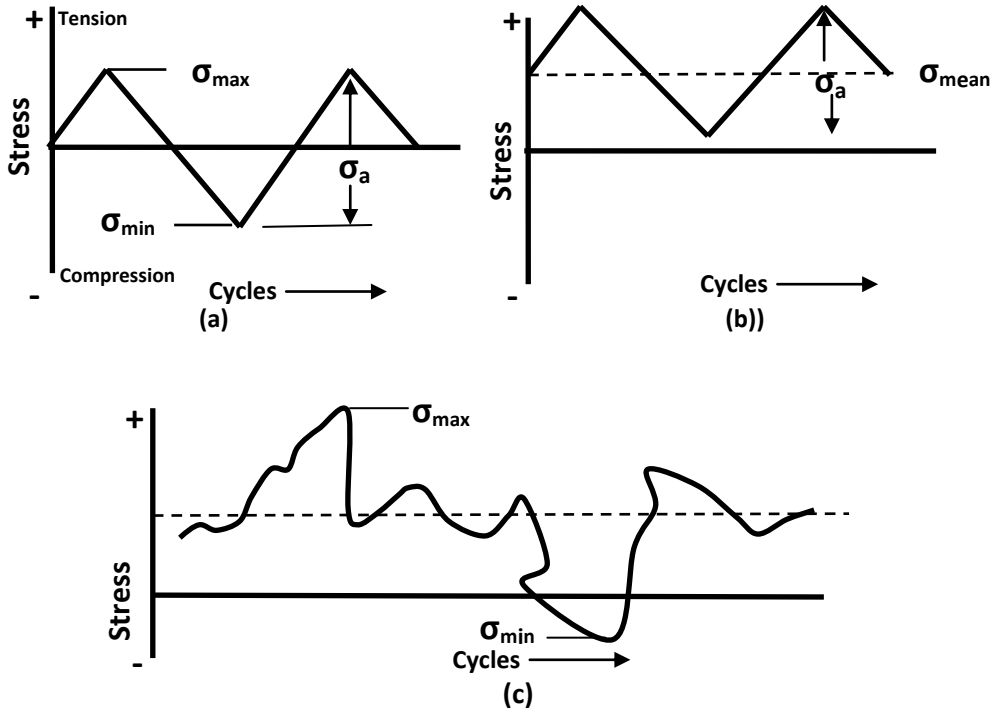

Fig. 2.1: (a) Reversed stress cycle (b) Repeated stress cycle (c) Irregular and random stress cycle.

2.2 Types of fatigue

Fatigue life plays an important characteristic in an engineering component which is measured by number of cycles it withstands before failure occurs. The mechanical fatigue can be divided into Low cycle fatigue (LCF) and high cycle fatigue (HCF). Generally failure occurs apparently by these two mechanisms. In LCF it involves some large loads along with relatively short lives where significant plastic strain occurs. But in HCF it is associated with lower loads and longer lives where stresses and strains are largely confined to the elastic region.

The main mechanism of LCF and HCF failures is that from stress concentrations (such as pores, inclusions etc.) there will be a local increase of stress levels due to pileup of dislocations, which will form slip bands and will grow to form cracks.

2.3 Low cycle fatigue

Low cycle fatigue is an important consideration in the design and operation of various components like aircraft, automotive and thermal power generating systems operating at high temperatures. These components experience cyclic loading and thermal stresses arising during thermal transients, which give rise to low cycle fatigue damage. Low cycle fatigue may be under stress controlled and strain controlled conditions as the surface region is constrained by the bulk of the component. Operating at high temperatures with steady load period introduces creep damage in the component materials. Hence the power plant components have to be designed as per fatigue, creep and its interaction effects.

2.4 Factors effecting LCF

Low cycle fatigue behavior of medium carbon steel depends on various factors like strain rate, temperature, strain ratio etc.

2.4.1 Effect of strain rate

Yang et al. [44] have studied about the high strain rate low cycle impact fatigue of medium carbon alloy 40Cr steel, at strain rate of $400s^{-1}$. They reported that the high strain rates in low cycle impact fatigue make the steel brittle and prone to early failure. Therefore low cycle impact fatigue is considered more dangerous than ordinary low cycle fatigue. Chandra et al. [45] investigated the effect of strain rate on low cycle fatigue behavior of 316L (N) stainless steel weld joints at strain rates of $3\times10^{-3}s^{-1}$, $3\times10^{-4}s^{-1}$ and $3\times10^{-5}s^{-1}$. They reported that initially brief hardening takes place; stress response at negative strain rate lowers the fatigue life, with decreasing strain rate. This has been correlated to dynamic strain aging regime operating at 823K. Based on fatigue mechanism relationship between time to failure and strain rate is used for life time prediction. Lee and Stone [46] reported the strain rate effect on LCF behavior of 63Sn/37Pb and showed that grain boundary sliding takes place at strain rates below $10^{-3}s^{-1}$ and caused the initiation of intergranualar cracks on the free surface of 63Sn/37Pb tensile test specimens.

Kanchanomai et al. [47] examined the strain rate effects on low cycle fatigue mechanism of eutectic Sn-Pb solder and they reported that in the low strain rate regime, wedge

cracking due to grain boundary sliding was the dominant mechanism. At high strain rate regime, extensive cavitations were observed on the colony boundary.

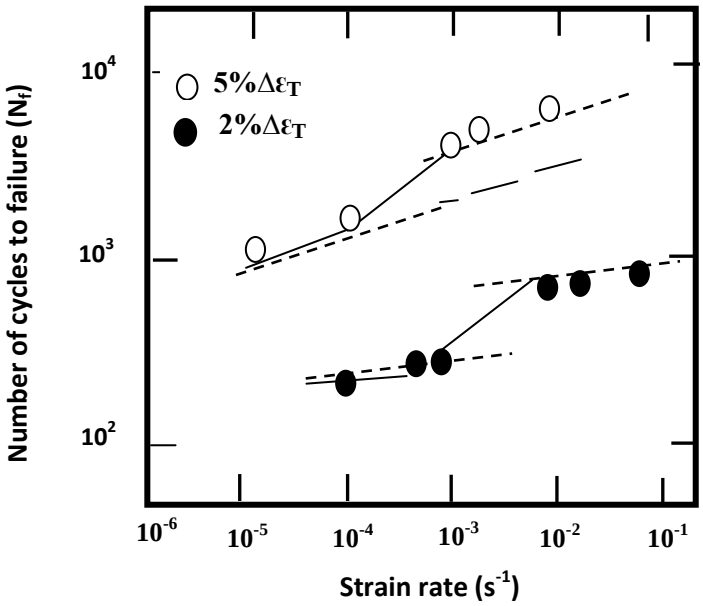

Fig. 2.2: Strain rate effect on number of cycles of eutectic Sn-Pb solder

The relationship between number of cycles to failure (N_f) and strain rate (s^{-1}) are shown in above Fig. 2.2. The reduction in the number of cycles to failure with decreasing strain rate can be observed for both 0.5% and 2% total strain ranges. Rong et al. [48] examined the effects of strain rate on low cycle fatigue behavior of high strength structural steel. They investigated the material in the strain rate at a range of 4×10^5 to 0.12 S^{-1}(0.001-3 Hz) under constant total strain control. The cyclic stress response at all strain rates exhibited behavior of rapid softening in the early stage of fatigue life and subsequent saturation up to failure.

2.4.2 Effect of strain amplitude

Xiong et al. [39] reported that extruded ZK60 magnesium (Mg) alloy under fully reversed strain controlled loading, dislocation slips dominate the cyclic plastic deformation when the strain amplitude is less than 0.35%. A typical feature is the symmetrical stress–strain hysteresis loops with zero mean stresses. When the strain amplitude ranges from 0.4% to 1.2%, partial twinning occurs under compression and detwinning occurs in the tensile reversal in a loading cycle. A distinct characteristic is the sustentation of the asymmetric

stress strain hysteresis loops and the positive mean stress with increasing loading cycles. When the strain amplitude is larger than 1.2%, the mean stress decreases quickly with increasing loading cycles and the stress–strain hysteresis loops tend to become more and more symmetric. Fatoba and Akid [49] observed strain amplitude effect on API 5L X65 Pipeline Steel at room temperature and reported that increasing the total strain amplitude results in decrease in LCF life and stress amplitude which is shown in Fig.2.3.

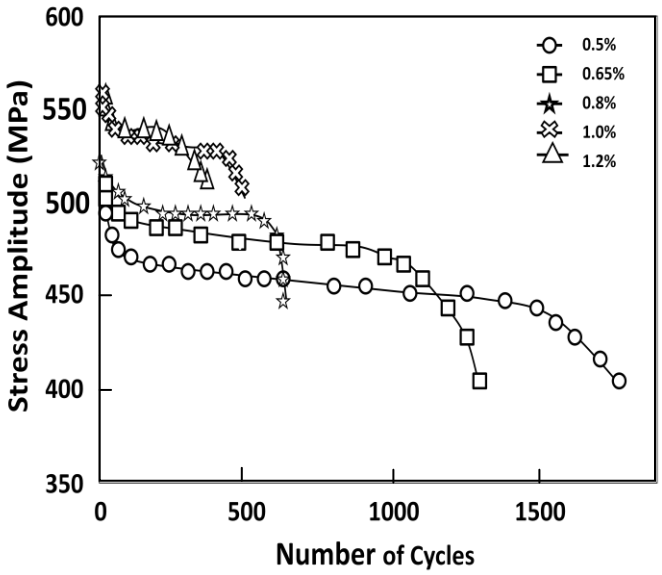

Fig. 2.3: Strain amplitude effect on number of cycles at different strain amplitudes of API 5L X65 Pipeline Steel

2.4.3 Effect of strain ratio

Hao et al. [50] have investigated on 2124-T851 Aluminium alloy for the low cycle fatigue tests with strain ratios of -1, -0.06, 0.06 and 0.5 under constant amplitude at room temperature; the material exhibited cyclic softening characteristic and the degree of softening decreased linearly with decreasing strain ratio. The lower fatigue life and ductility of the material corresponded to the larger strain ratios. The substructural observations revealed that the density and length of slip bands increased with increasing strain ratios. Begum et al. [51] reported LCF behavior of AZ31 wrought magnesium alloy. The evolution of stress amplitude during cyclic deformation is shown in Fig.2.4. It shows that the material exhibited higher cyclic hardening at the lower (or more negative) strain

ratio than at the higher strain ratio, and at R = 0.5 the cyclic hardening became much weaker and almost linear in the semi-log coordinate. The stress amplitude also increased with increasing R values under the same strain amplitude and strain rate. The residual twins acting as barriers to dislocation slip and thus pileup of dislocations were considered to be the main cause for the occurrence of cyclic hardening. Fatigue life increased with decreasing strain ratio and increasing strain rate.

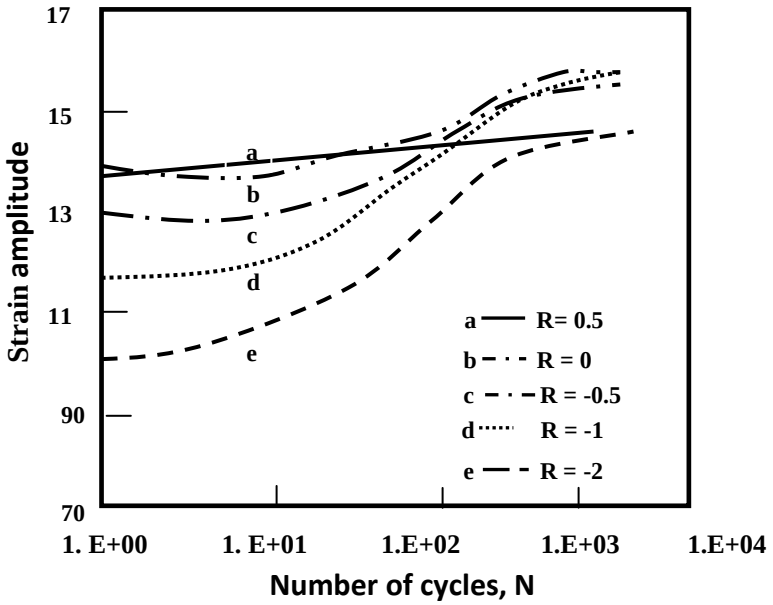

Fig. 2.4: Strain amplitude vs. number of cycles at different strain ratios R.

Wang et al. [52] reported that the welded joints of Ti-6Al-4V base metal and Ti17 base metal basically exhibited asymmetrical hysteresis loops in tension and compression in the fully reversed strain controlled tests. At a strain ratio of R_e= 0 &0.5, a large amount of plastic deformation occurred in the ascending phase of the first cycle of hysteresis loops of Ti-6Al-4V BM, Ti17BM due to the high positive mean strain values. Fatigue life was observed to be longest at R_e= -1 and it is decreased as the strain ratio deviated from R_e= -1.

2.4.3 Effect of temperature

Guocaichai et al. [53] investigated about the low cycle fatigue properties of Ni base alloys and they reported that at high temperature micro twins were initiated in Ni based alloy,

which increased the plasticity and contributed to most of the localized deformation and consequently the softening. If only plastic strain is concerned, the influences of strain amplitude on the fatigue properties at room temperature and 204^{o}C temperatures are comparable (Fig. 2.5 a). The cyclic stress-strain responses at these two temperatures, however, vary differently. At room temperature, alloy 690 shows a normal cyclic hardening and softening response. Increase in strain amplitude increases both hardening and softening rate. At 204^{o}C, however, the stresses in the beginning increase with increasing number of cycles as expected.

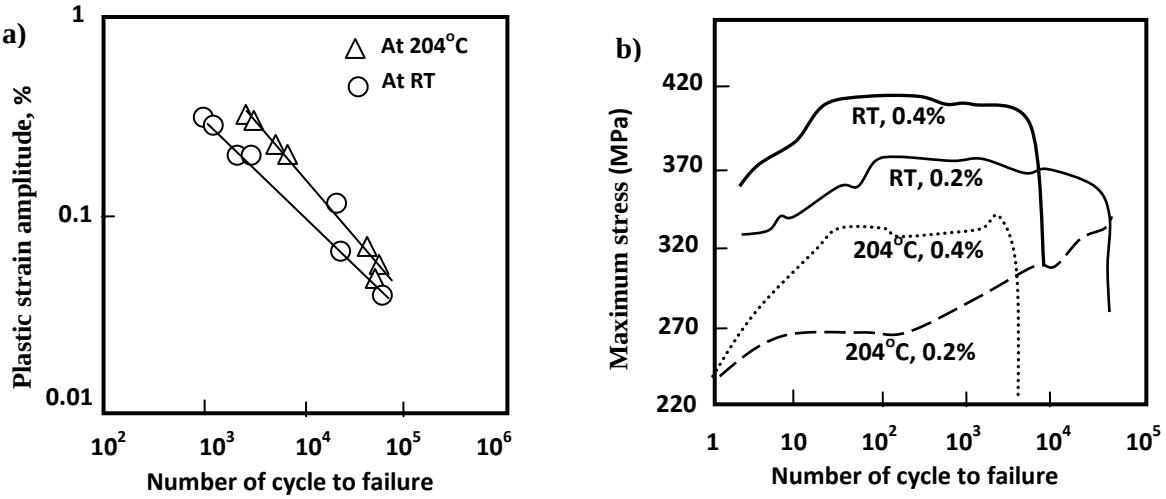

Fig. 2.5: (a) Strain amplitude vs. fatigue life (b) Cyclic stress response under strain controlled fatigue at RT and 204^{o}C for alloy 690 material.

Grzegorz and Mrozinski [54] have extensively studied the fatigue behavior of cast steel and concluded that there is a growth of the mean diameter of $M_{23}C_6$ carbides at high temperature. He considered that the $M_{23}C_6$ carbide coarsening growth of mean diameter of sub grains and decrease in dislocation density and also disappearance of lath morphology are believed to be dominant factors for acceleration of fatigue softening of G×12CrMoVNbN9-1 cast steel. Zettle et al. [55] reported the very high cycle fatigue behavior of normalised carbon steel at room temperature constant amplitude cyclic loading. At low number of cycles, the material deformation is almost purely elastic, since dislocation in the ferrite grains and in the ferrite of the pearlite is blocked by carbon atoms. Then dislocation mobilization starts and cyclic softening connected with a localization of

plastic strain is observed. Srinivasan et al. [56] examined the low cycle fatigue behavior of nitrogen alloyed type 316L stainless steel; the cyclic stress response at all temperatures was characterized by an initial hardening to the maximum stress, followed by gradual softening prior attaining saturation. Temperature dependence of fatigue life showed a maximum in the intermediate temperature range. Kim et al. [57] have done the analysis on high temperature low cycle fatigue properties of 24Cr ferritic stainless steel and concluded that the fatigue strength of 24Cr stainless steel decreased with increasing temperature but the fatigue life increased at 600°C and 700°C. The fatigue behavior at room temperature was characterized as cyclic hardening followed by saturation and cyclic softening while marginal cyclic hardening was observed at 600°C and 700°C which was shown in Fig 2.6. Microstructural analysis showed that persistent slip bands developed prevalently at room temperature but not at 600°C and 700°C.

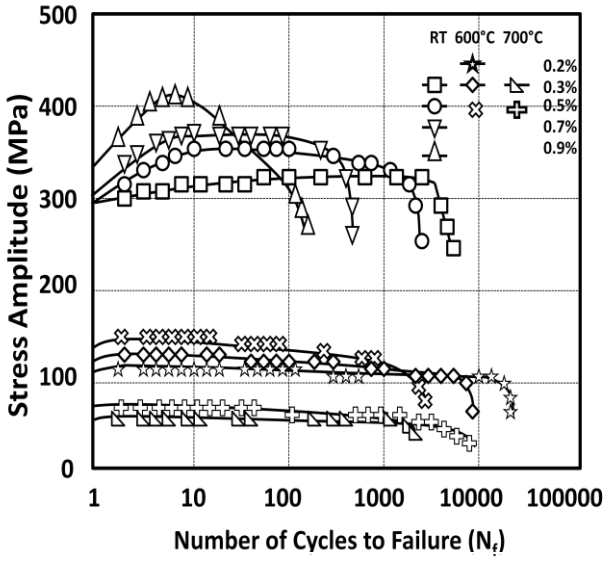

Fig. 2.6: Cyclic stress response curve of 24Cr ferritic stainless steel at RT, 600^{o}C and 700^{o}C.

2.5 Ratcheting

Ratcheting, a cyclic accumulation of inelastic deformation will occur in the materials subjected to a stress-controlled cyclic loading with non-zero mean stress [30-37]. It is a cyclic plastic strain accumulation process which takes place in engineering components

when they are subjected to asymmetrical cyclic stress and it greatly depends on type of materials. Ratcheting deformation occurs in such a way that the hysteresis loops produced for subsequent cycles translate towards higher plastic strain direction. This phenomenon illustrated in Fig. 2.7 and briefly explained in Fig. 2.8.

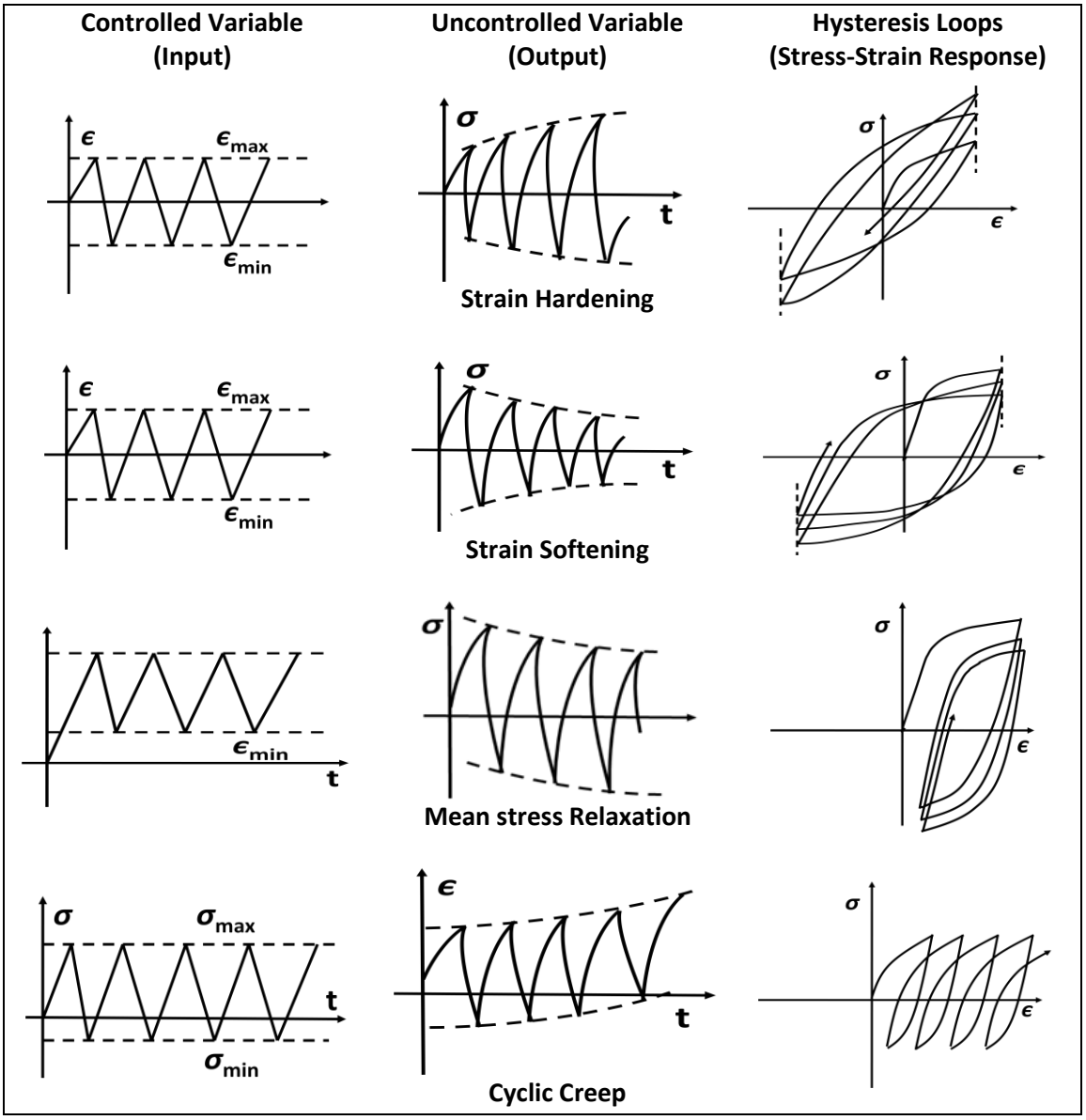

Fig. 2.7: Material response to various modes of cyclic input variables (stress controlled).

Rings berg [2001] has stated that instances where the material shows additional plastic deformation for every load cycle are known as ratcheting. The accumulation of deformation continues until the material ductility is exhausted. The rate of strain accumulation continuously decreases with increasing number of cycles, indicating material response towards a steady state.

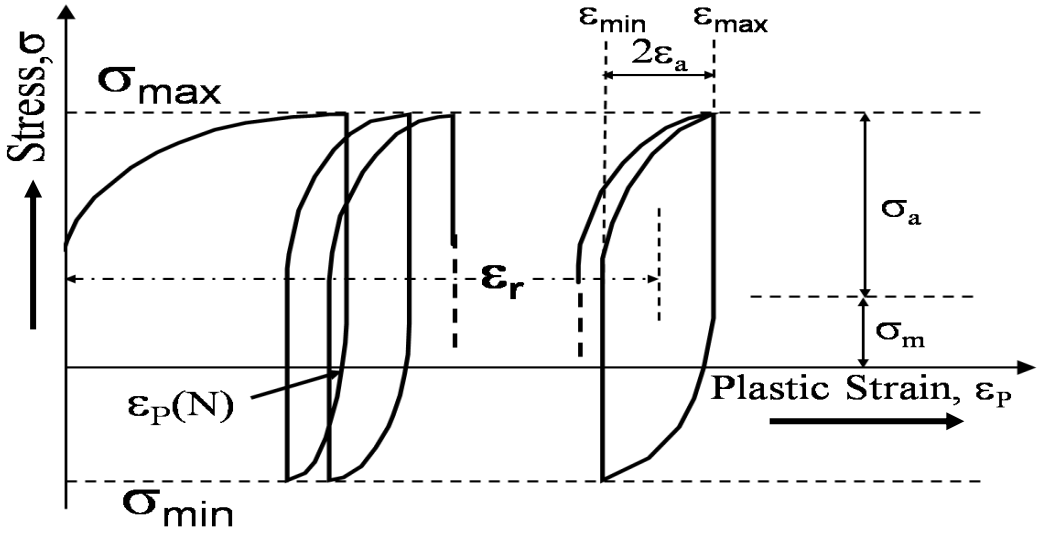

Where,

σ_{max} = Maximum stress σ_{min} = Minimum stress

σ_m = Mean stress σ_a = Stress amplitude

Fig. 2.8: Schematic illustration of ratcheting

Numerically, ratcheting strain is measured as the mean strain for a particular cycle and it is expressed as:

$$\varepsilon_r = (\varepsilon_{max} + \varepsilon_{min})/2$$

Where,

ε_r = ratcheting strain

ε_{max}= maximum strain at a particular cycle

ε_{min}= minimum strain at the cycle.

2.6 Factors effecting ratcheting

Strain accumulation by ratcheting limits the predictive capability of well-known Coffin Mansion relation [1] and it is known that accumulation of ratcheting strain usually degrades fatigue life of structural components [2, 3]. The extent of degradation depends on the imposed stress parameters such as mean stress, stress amplitude, stress ratio etc. and the nature of the material.

2.6.1 Effect of mean stress and stress amplitude

Several group of researchers have reported that strain get accumulated during ratcheting is due to presence of positive or negative mean stress. Dutta and Ray [23] reported that the accumulation of ratcheting strain for interstitial free steel increases if the magnitude of stress amplitude gets increased from 130 to 150 MPa at constant mean stress. Similar orders of increase in strain accumulation are observed with increase in mean stress, for any constant value of stress amplitude. These variations are illustrated in Fig. 2.9.

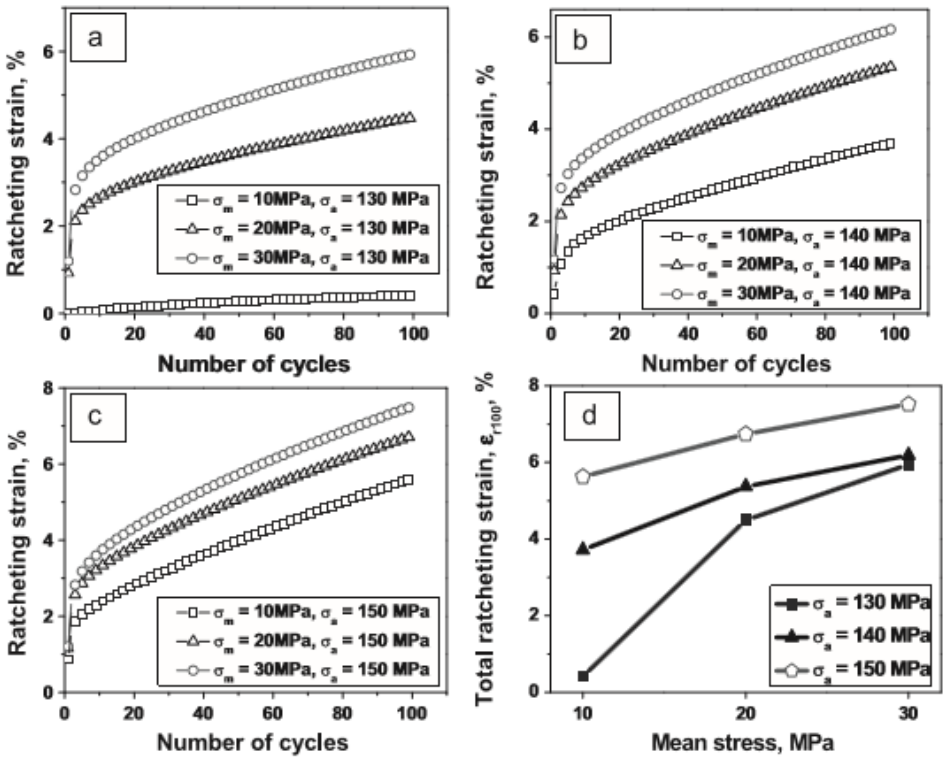

Fig. 2.9: Variation of ratcheting strain with no. of cycles for varying mean stresses and at constant stress amplitude of (a) 130 MPa, (b) 140 MPa, (c) 150 MPa and (d) total accumulation of ratcheting strain.

Researchers also studied the effect of positive to negative mean stress on the nature of strain accumulation of copper alloy and reported that accumulation of strain due to ratcheting positive for positive mean stress and are negative for negative mean stress [23]. In case of constant stress amplitude, both ratcheting life and strain accumulation increase with tensile mean stress. In case of tensile and compressive mean stress, strain accumulation paths are mirror of each other. Ratcheting strain amplitude and ratcheting strain rate 63Sn37Pb increases with increase in stress amplitude or mean stress correspondingly [46, 47 and 58].

2.6.2 Effect of stress ratio

Stress ratio ($R = \sigma_{min}/\sigma_{max}$) acts as an important parameter during asymmetric cyclic loading of a material. The effect of stress ratio on the nature of the accumulation of ratcheting strain has been reported by a few investigators [15, 59-60]. Yoshida [21] reported that significant strain accumulation can take place when R is both positive and negative. When R= -1, mean stress is zero, which indicates, symmetric cyclic loading. Hence there is almost negligible strain accumulation for R= -1. Plots of ratcheting strain *vs.* number of cycles for various R ratios are as shown in Fig. 2.10.

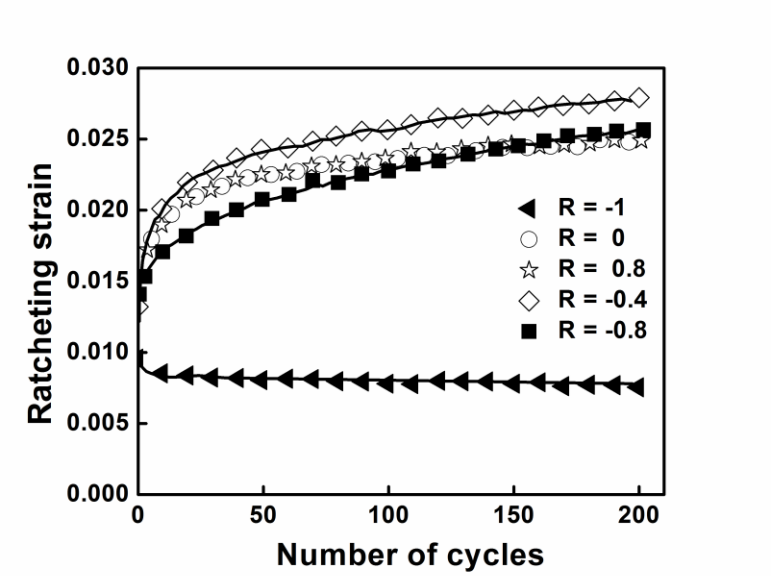

Fig. 2.10: Variation of ratcheting strain with number of cycles for varying stress ratios of -1, 0, 0.8, -0.4 and -0.8.

The plots for R = 0 and R = 0.8 show almost similar amount of strain accumulation. Thus it may be considered that the strain accumulation due to ratcheting does not vary with increase in the magnitude of R. Shivaprasad et al. [59] worked on effect of stress ratio on strain accumulation due to ratcheting for SA 333 group 6 piping steel. The results indicate that strain accumulation does not take place upto R = -0.25, while it is significant for R= -0.50 and -0.75. Hence, they reported that stress ratio should be sufficiently negative for ratcheting to occur.

Kang et al. [32] explained (Fig. 2.11) the ratcheting behavior of tempered 42CrMo steel under stress controlled cyclic loading with various peak stresses and stress ratios. It is seen from Fig. 2.11 that most significant ratcheting occurs at the stress ratio of -0.889; increasing stress ratio results in reduction in strain accumulation. When the peak stress is kept constant at 800 MPa and 900 MPa, the ratcheting strain observed is very less at relatively high stress ratio of -0.500 and -0.444 respectively [15].

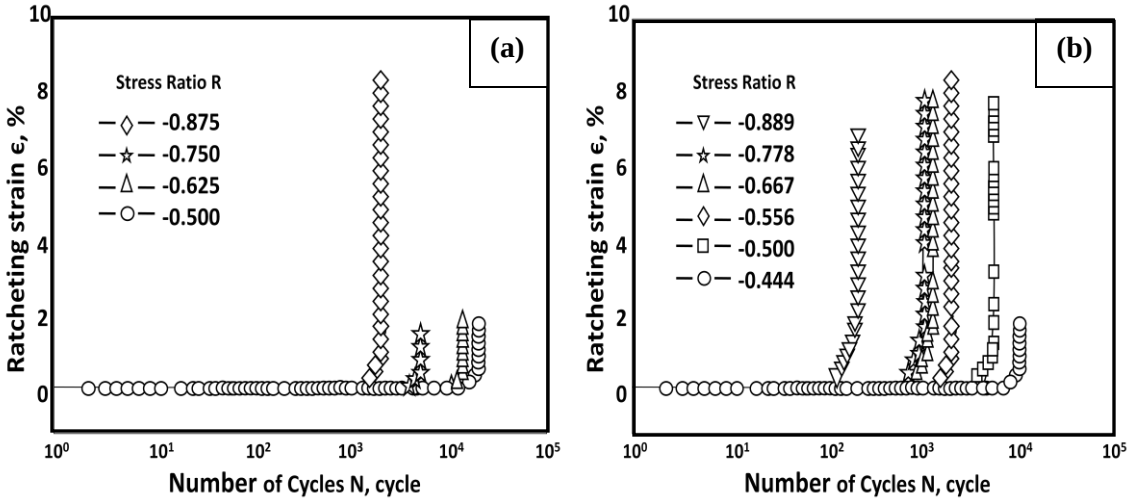

Fig. 2.11: Relation between ratcheting strain vs. number of cycles for (a) for peak stress 800 MPa (b) for peak stress 900 MPa.

2.6.3 Effect of temperature

Kang et al. [2] reported that at room and elevated temperatures, the ratcheting behavior of SS304 stainless steel depends on the temperature. The ratcheting strain increases with the

mean stress and stress amplitude. Under the stress cycling with variable mean stresses and constant stress amplitude, at room temperature, as shown in Fig. 2.12 (a), when mean stress is small (for case 1), ratcheting does not occur during the cycling. As the mean stress is high enough (for case 2), the ratcheting occurs. The ratcheting strain increases with the increasing of mean stress.

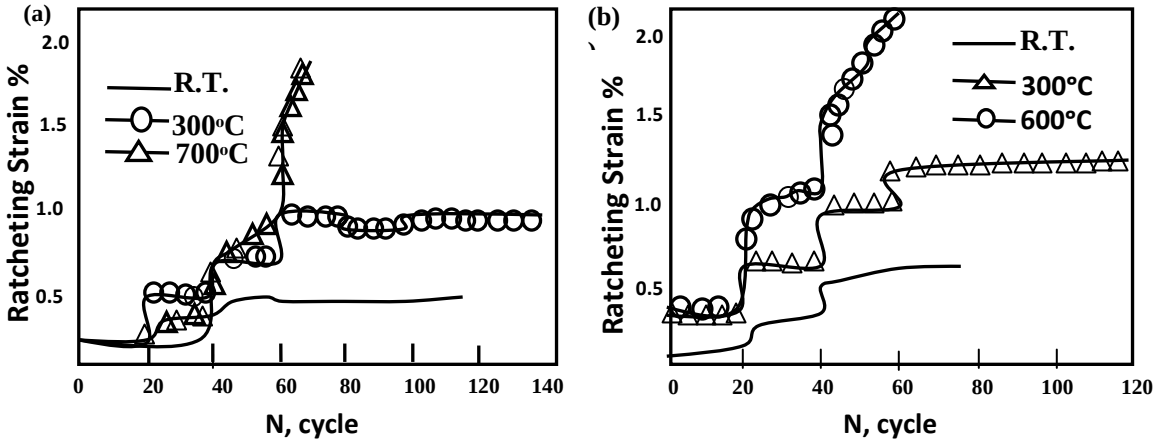

Fig. 2.12: Ratcheting strain vs. number of cycles under (a) constant strain amplitude (b) constant mean stress.

Under the stress cycling with variable stress amplitudes and constant mean stress, at room temperature, the ratcheting strain and its rate increase with the stress amplitude. At high temperatures, as shown in Fig. 2.11(b), the ratcheting strain has the same variations as those at room temperature with respect to stress amplitude and number of cycles N. However, though the stress level of each loading case at high temperatures is lower than that at room temperature, the ratcheting is more considerable. It can be obtained that the ratcheting strain increases with the ambient temperature.

2.6.4 Effect of cyclic hardening and softening features

Generally materials presented in the stress cycling by addressing the cyclic softening/hardening feature of the material. Ratcheting behavior of a material depends on cyclic hardening/ softening features of it. Paul et al. [27] reported that hardening of the material during cyclic deformation can be explained in the ways like, decrease in the size of hysteresis loop/hysteresis loop area or decrease in the width of hysteresis loop. Sarkar et

al. [9] reported that the hardening associated with increase of mean stress and the corresponding lowering of absorbed cyclic plastic strain energy per cycle increases the ratcheting fatigue life. Ratcheting curves of solution annealed austenitic stainless steel (ASS) as shown in Figure 2.13 (a) and (b) reveal the ratcheting strain accumulation pattern in the specimen as a function of number of cycles (N) at 1100°C and 1200°C. They concluded that when the material ASS under cyclic hardening behavior, the ratcheting strain decreases with increasing number of cycles.

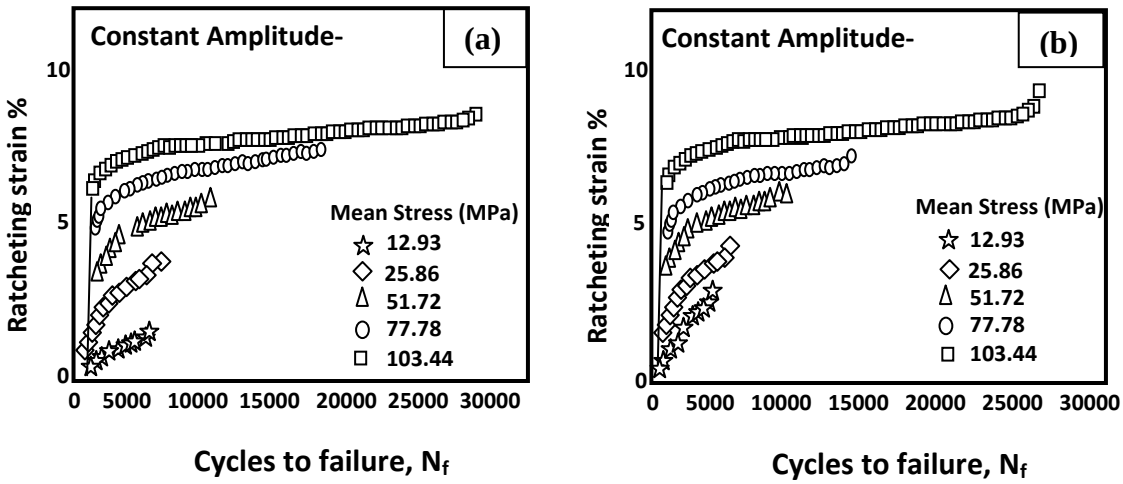

Fig. 2.13: Ratcheting curves showing the strain evolution pattern with progression of cyclic loading of the investigated 304 austenitic stainless steel annealed at (a) 1100°C (b) 1200°C.

2.7 Structural features of fatigue

The process of damage accumulation due to cyclic loading of a metal is complex. The structural variations of a metal subjected to cyclic loading can be divided into the following stages:

1. Crack initiation
2. Slip band crack growth
3. Crack growth on planes of high tensile stress
4. Ultimate ductile failure.

Fatigue cracks initiate at a free surface before 10 percent of the total life of the specimen has elapsed. Slip lines are formed during the first few thousand cycles of stress and

successive cycles produce additional slip bands. Cracks usually occur in the region of heavy deformation. There are several slip bands which are more persistent than the rest and which will remain visible when the other slip lines have been polished away. These persistent slip bands are embryonic fatigue cracks since they open into wide cracks on the application of small tensile strains.

Initiation of fatigue deformation is the formation of ridges and grooves called slip band extrusions and intrusions on the surface. These micro deformations lead to the formation of fatigue crack, as these serve as regions of high stress concentrations. The mechanism for the initiation of fatigue crack is in agreement with the facts that fatigue cracks start at surfaces and cracks have been found to initiate at slip band intrusions and extrusions.

2.8 Fatigue life prediction: Total life and safe life approach

By means of stress strain based wholer diagram the approximate number of cycles can be predicted upto which a component can be used until a failure criteria is reached, either defined as complete fracture or by exceeding a critical crack length or maximum strain according to dimensioning of the wholer system. The strain based Wohler diagram (Fig.2.14) can be described mathematically by superimposing basquins equation for HCF regime ($N_f > 10^4$ cycles) and Monson's and coffin's equation for LCF regime ($N_f < 10^4$ cycles). Taking the detrimental effect of a mean stress into account the superimposition yields the following relationship between the total strain amplitude and the number of cycles to technical crack initiation N_f.

$$\frac{\Delta\varepsilon}{2} = \frac{\Delta\varepsilon_e}{2} + \frac{\Delta\varepsilon_p}{2} = \frac{\sigma_f - \sigma_o}{E}\left[2N_f\right]^b + \varepsilon_f\left[2N_f\right]^c$$

The strain based Wohler diagram can be approximated by data from monotonic tensile tests using the ultimate tensile tests using the ultimate tensile strength.

$$\varepsilon_f = \frac{\text{Original specimen cross section}}{\text{Cross section after fracture}}$$

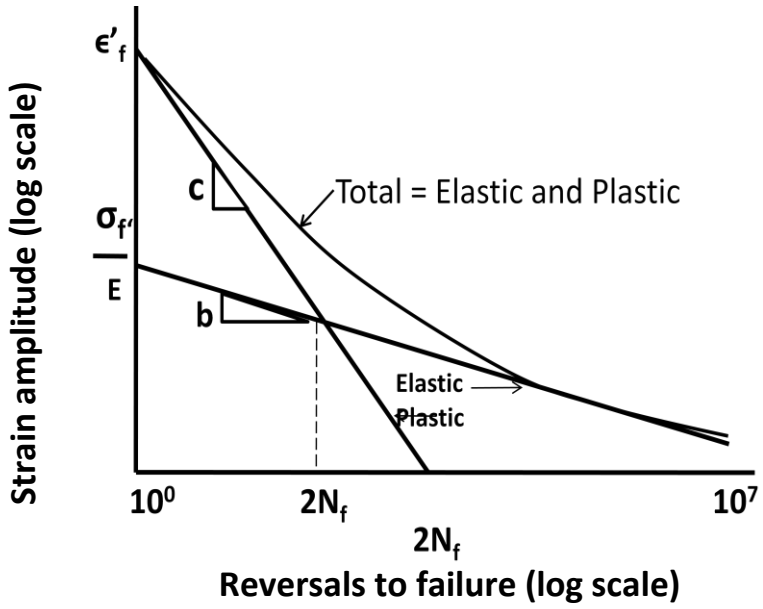

Fig. 2.14: Fatigue strain life curve obtained by super position of elastic and plastic strain life equations (schematic).

CHAPTER 3

EXPERIMENTAL PROCEDURES

EXPERIMENTAL PROCEDURES

3.0 Introduction

The aim of this investigation is to study the cyclic deformation behavior of AISI 4340 steel, in conjugation with the investigations related to grain size effect on ratcheting behavior. To fulfill these aims, various kinds of experiments were conducted which are described in this chapter. An overview of all the experiments includes determination of chemical composition of the selected steel, heat treatment, microstructural analysis, determination of tensile behavior of the steel, study of fracture surfaces, experiments related to stress-controlled and strain controlled fatigue behavior, X-ray diffraction studies, scanning electron microscopy and pre and post fatigue hardness tests.

3.1 Material selection and specimen specification

The sample selected for the current investigation was a medium carbon steel designated as AISI 4340. It is one of the American standard specifications of the medium carbon steel having the ferrite matrix with pearlite and so it has high toughness and strength [38]. This steel is selected due to wide applications like designing components of aircrafts (crank shafts, gears and engine parts) and other machinery parts etc. and these components experience fatigue type of load on service. The steel was available in the form of rods of 18 mm diameter. The chemical composition of the selected material has been assessed using optical emission spectrometer.

3.2 Heat treatment

Steels can be heat treated to produce a great variety of microstructures and properties. One of the objectives of this study is to investigate the effect of grain size on low cycle fatigue behavior of the material associated with ratcheting deformation. Therefore the steel has been subjected to two types of heat treatments viz. annealing and normalising. In this investigation the steel has been heat treated using electric pit furnace. One set of specimens have been heated up to 750°C and at this temperature these were held for 2 h. for soaking.

After soaking, these were cooled slowly to facilitate annealing operation. Another set of specimens have been heated up to 877°C, after soaking of 2 h. these has been taken out of the furnace to allow these to cool in air to facilitate normalising operation Figure 3.1 (a) shows furnace cooled samples after annealing and Fig.3.1 (b) shows the air cooling of specimens during normalising.

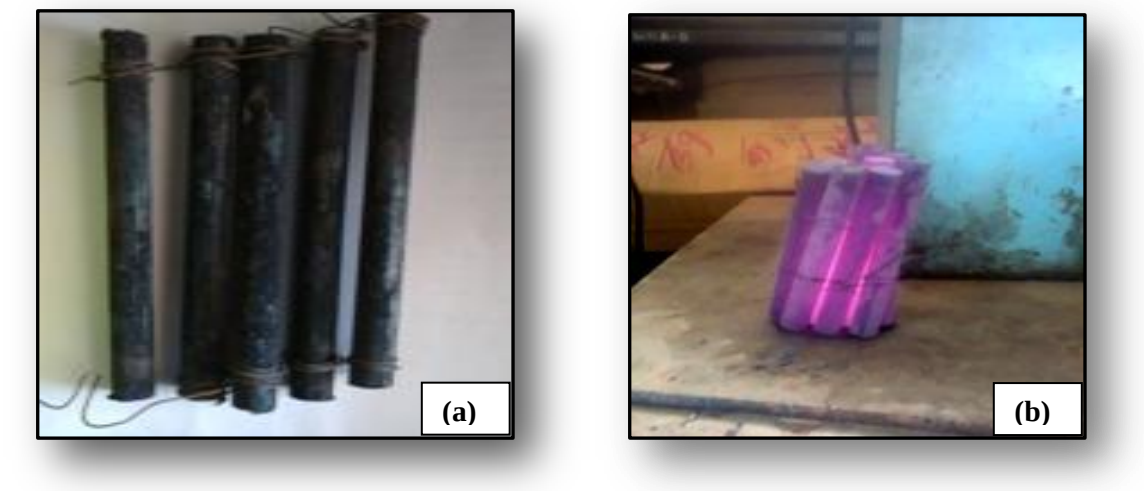

Fig. 3.1: (a) Annealed samples after cooled to room temperature (b) Normalised samples during cooling

3.3 Specimen design for tensile and fatigue tests

Tensile and fatigue test specimens have been fabricated as per ASTM standards E8M [61] and E-606 [62] respectively from heat treated rods of 220 mm length. Typical configurations of tensile and fatigue specimens are shown in Fig. 3.2 (a) and (b). Snapshot of actual tensile and fatigue specimens also shown in Fig. 3.2 (c).

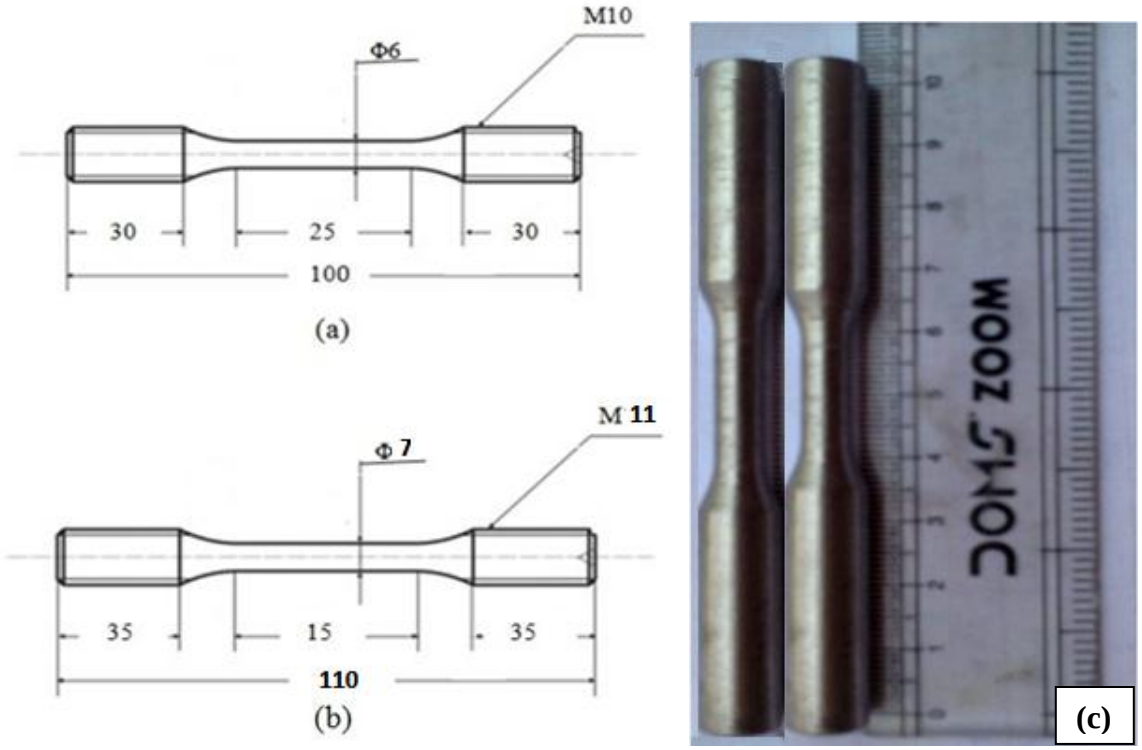

Fig. 3.2: (a) Typical configuration of tensile specimen (b) Fatigue specimen and (c) snapshot of actual tensile and fatigue specimens

3.4 Microstructural analysis and grain size measurement

Samples of approximately 10 mm diameter with 8 – 10 mm height have been cut from heat treated steel for metallographic examinations. All specimens have been initially thoroughly polished using emery papers of 1/0, 2/0, 3/0 and 4/0 grades and finally using 0.25 µm diamond paste and etched with suitable etchant, nital (2% HNO_3 and 98% ethanol). The microstructural constituents of the investigated steel have been examined using an optical microscope (Carl Zeiss, model no.: 3327000403, Germany) connected to an image analyzer (Software: Axio vision release 4.8 S.P 3) and a series of representative photographs have been recorded. The microstructure of the investigated steel exhibited larger grains for annealed samples and smaller grains for normalised ones.

The average grain size has been estimated using linear intercept method following ASTM standard E-112 [63]. In this method, a linear test grid has been superimposed on the microstructure and the number of grains intercepted by the test line has been counted. Such measurements have been repeated at least on 50 randomly chosen fields. The grain size (d) has been calculated as:

$$d = \frac{L_T}{N_L}$$

Where, N_L = No. of grains intercepted by a unit true test line length. The true length L_T of a test line is defined as the length of the test line at unit magnification.

3.5 Study of mechanical properties

3.5.1 Hardness testing

Hardness is defined as the ability of a material to resist plastic deformation, usually by indentation. The specimens for hardness measurements have been first ground flat and parallel to each other using a belt grinder to ensure accuracy of measurements. Then the samples mechanically polished as mentioned in section 3.4. Using Vickers hardness tester (LECO LV400, US), the hardness has been measured at a load of 20 kgf with dwelling time of 15s. At least 3 readings have been taken on each specimen for the estimation of average hardness values.

3.5.2 Tensile test

The most common type of test used to measure the mechanical properties of a material is the tension test. This test is widely used to provide basic design information on the strength of materials. In this investigation servo hydraulic universal testing system (BISS, ±100kN, India) is used to perform the test. Round bar specimens, having gauge length 25 mm and diameter 10 mm have been fabricated from annealed and normalised rods according to ASTM standard E8M [61]. Gage portion of the specimens have been polished by holding these in lathe machine to make surface flaw free and make the smooth using fine grade emery papers. Tensile test has been performed at cross head speed of 1mm/min. For each

test, the load displacement values have been automatically recorded for subsequent processing.

3.5.3 Fatigue test

Stress controlled and strain controlled fatigue tests have been carried out at room temperature. Stress-control tests have been done at a constant stress rate of 50 MPa/s and strain controlled tests at a strain rate of 0.08 s^{-1}. Based on the employed test controls, the test can be classified into three categories (i) Ratcheting by varying stress ratios (ii) LCF followed by ratcheting (iii) Ratcheting followed by LCF.

3.5.3.1 Ratcheting by varying stress ratios

Ratcheting (stress controlled) tests have been done at stress ratios of -0.4, -0.6 and -0.8. The maximum stress selected as 80% of ultimate tensile strength i.e., 800 MPa and 1300 MPa for annealed and normalised specimens respectively. All these details are listed in Table 3.1.

Table 3.1: Test matrix for ratcheting test under varying stress ratios.

S. No.	Stress ratio (R)	Annealed		Normalised	
		σ_a (MPa)	σ_m (MPa)	σ_a (MPa)	σ_m (MPa)
1	-0.4	560	240	910	390
2	-0.6	640	160	1040	260
3	-0.8	720	80	1170	130

During each test, the load- extension as well as the actuator displacement data has been continuously recorded by using the attached software to the computer. It was aimed to acquire at least 250 data points per cycle during test. All fatigue tests have been done upto

100 cycles and then post ratcheting tensile test has been done for further analysis on these samples.

3.5.3.2 LCF followed by Ratcheting

One set of annealed specimens have been studied for strain controlled low cycle fatigue test upto 100 cycles and for another set of specimens strain controlled test has been done after ratcheting (stress controlled). All these details are listed in Table 3.2. Strain controlled test has been done at strain rate of 0.08 s^{-1} and strain amplitudes of ±0.25 and ±0.50. Ratcheting test has been done at fixed maximum stress of 800 MPa. Load-extension as well as the actuator displacement data has been recorded and finally result compared between only LCF and after ratcheting LCF in terms of stress amplitude.

Table 3.2: Test Matrix for LCF followed by Ratcheting Test.

S. No.	Only LCF	LCF followed by Ratcheting	
		Ratcheting	**LCF**
1	Strain amplitude of ±0.25	σ_a=560 MPa, σ_m=240 MPa	Strain amplitude of ±0.25
2	Strain amplitude of ±0.50	σ_a=560 MPa, σ_m=240 MPa	Strain amplitude of ±0.50

3.5.3.3 Ratcheting followed by LCF

One set of annealed specimens have been tested for ratcheting test done upto 100 cycles and for another set of specimens have been tested for ratcheting after strain controlled LCF test up to 100 cycles. All the details of these tests are listed in Table 3.3. All ratcheting and strain controlled tests have been done as mentioned in section 3.5.3.2. Load-extension as well as the actuator displacement data has been recorded and finally results are compared in terms of ratcheting strain between only ratcheted and after LCF ratcheted specimens.

Table 3.3: Test matrix for ratcheting followed by LCF test.

S. No.	Only Ratcheting	Ratcheting followed by LCF	
		LCF	**Ratcheting**
1	σ_a=560 MPa, σ_m=240 MPa	Strain amplitude of ±0.25	σ_a= 560 MPa, σ_m= 240 MPa
2	σ_a=560MPa, σ_m=240 MPa	Strain amplitude of ±0.50	σ_a= 560 MPa, σ_m= 240 MPa

3.6 Post ratcheting tensile and fractography

Post ratcheting tensile test has been done for ratcheted specimens to know the yield strength and ultimate tensile strength variations after the ratcheting. For this study the tensile tests have been done as mentioned in section 3.5.2. To study the fracture surface, transverse sections from the gauge portion of the broken tensile and post ratcheting tensile specimens have been cut. Figure 3.3 shows the fractured specimens after tensile test.

Fig. 3.3: Typical configuration of fractured specimens of tensile and post ratcheting tensile samples of investigated steel.

Images of the fracture surface have been taken by scanning electron microscope (SEM) at different magnifications. The instrument model used for the SEM analysis was JEOL JSM-5800LV. A potential of 20 KV has been used for the scanning electron microscope and the magnification used for the samples are 2000X respectively. Compositional analysis on the sample has been carried out by the energy dispersive spectroscopy (EDS) attached with the SEM. The EDS normally reveals the presence of elements at inclusions.

3.7 XRD profile analysis

The X-ray diffraction profile analysis (Model: XPert-3040Y00, Holland) using the modified Williamson–Hall equation has been carried out in order to estimate the dislocation density in the specimens subjected to both strain controlled and ratcheting deformation. For this study the samples has been cut below fracture surface, transverse sections from the gauge portion of the broken tensile and post fatigue loaded specimens. These analyses were carried out using high resolution Cu-Kα radiation. Samples were subjected to XRD in the scanning range of 30°-110° at scanning rate of 5°/min. The results will be compared in terms of dislocation densities between undeformed and low cycle fatigue loaded specimens.

3.8 Post-ratcheting hardness

Post-ratcheting hardness tests have been done by cutting the transverse sections of the gauge portion of the ratcheted samples with approximate height of 10 mm, after cutting the portion containing the fracture surface. Specimens have been prepared for hardness studies as mentioned in Section 3.4.1.

CHAPTER 4

RESULTS AND DISCUSSION

RESULTS AND DISCUSSION

4.0 Introduction

The aim of this investigation is to study the low cycle fatigue (LCF) behavior of AISI 4340 steel particularly under stress controlled and strain controlled conditions. To fulfill this aim various experiments have been conducted, which are described in chapter 3. This chapter deals with the obtained results of all the experiments conducted during this investigation in association to their brief discussion. This chapter is divided into various sub-sections: Section 4.1 deals with chemical analysis of the investigated steel; In Section 4.2 microstructural analysis and grain size result have been discussed; results of mechanical properties includes results and discussion of uniaxial ratcheting tests and strain controlled fatigue test have been provided in Section 4.3 with relevant discussion, Sections 4.4 to 4.7 includes, post ratcheting tensile, post ratcheting hardness variations, fractographic features of the broken tensile sample, XRD profile analysis results respectively.

4.1 Chemical analysis

The chemical composition of the selected material which was obtained using optical emission spectrometer is shown in the table 4.1. The AISI 4340 steel contains around 0.35 - 0.38% C with Ni, Cr and Mo as chief alloying elements. The presence of 1.52% Ni, 1.44% Cr and 0.18% Mo are at per with the composition of AISI 4340 steel, as per ASM handbook [38].

Table 4.1: Chemical composition of AISI 4340 Steel.

Element	C	Si	Mn	S	P	Cr	Ni	Mo	Al	Fe
Wt.%	0.35	0.31	0.69	0.02	0.03	1.44	1.52	0.18	0.03	Balance

Among all the alloying elements in AISI 4340 steel, the presence of nickel in low alloy steels increases the toughness and hardenability. Molybdenum ensures uniform microcrystalline structure and augments hardenability and high temperature tensile strength whereas the presence of chromium improves toughness, hardness and wears resistance.

4.2 Microstructural analysis and grain size measurement

The optical microstructures of the investigated material under annealed and normalised conditions are shown in Fig. 4.1 and Fig. 4.2. The annealed microstructure in Fig. 4.1 (a) shows the ferrite (light) and pearlite (dark).

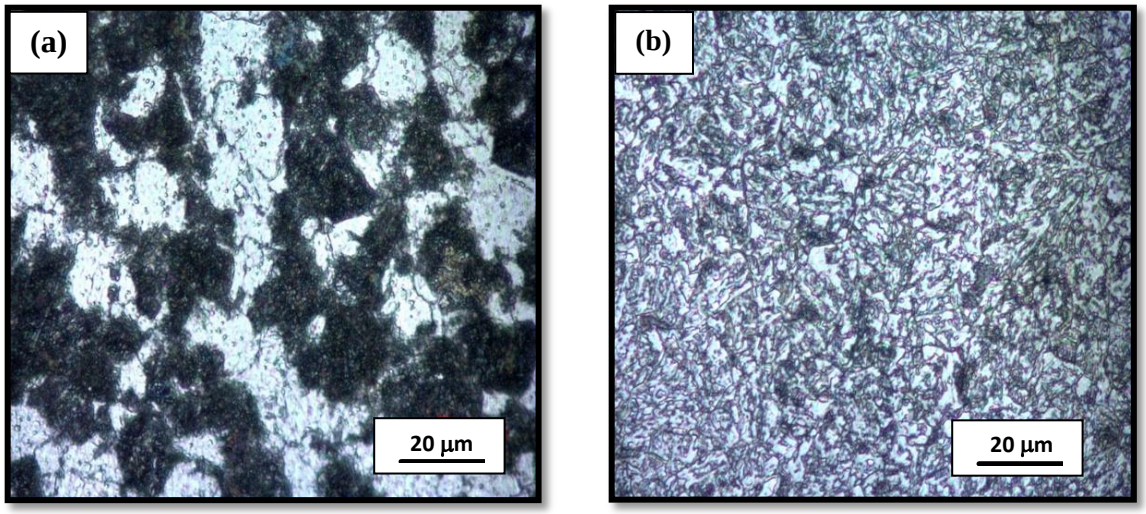

Fig. 4.1: Optical microstructure of (a) annealed (b) normalised AISI 4340 steel at 100X magnification.

Figure 4.1 (b) shows the optical microstructure of normalised AISI 4340 steel at 100 X magnifications and Fig. 4.2 (b) shows typical SEM microstructure at 1000X magnification which shows the soft ferrite (light) and pearlite (dark) phases. The normalised microstructure shows finer grain size as compared to the annealed microstructures. The faster rate of cooling during normalising process has lead to the formation of finer grain size as grain growth occurs during slow cooling in annealing process [38]. Typical SEM

images of annealed and normalised specimens of investigated steel are illustrated in Fig. 4.2. Grain size obtained by using linear intercept method according to ASTM standard E112 [63]. Average grain size of the specimen was found to be 16.55±2.07µm and 7.20±1.15µm for annealed and normalised samples respectively.

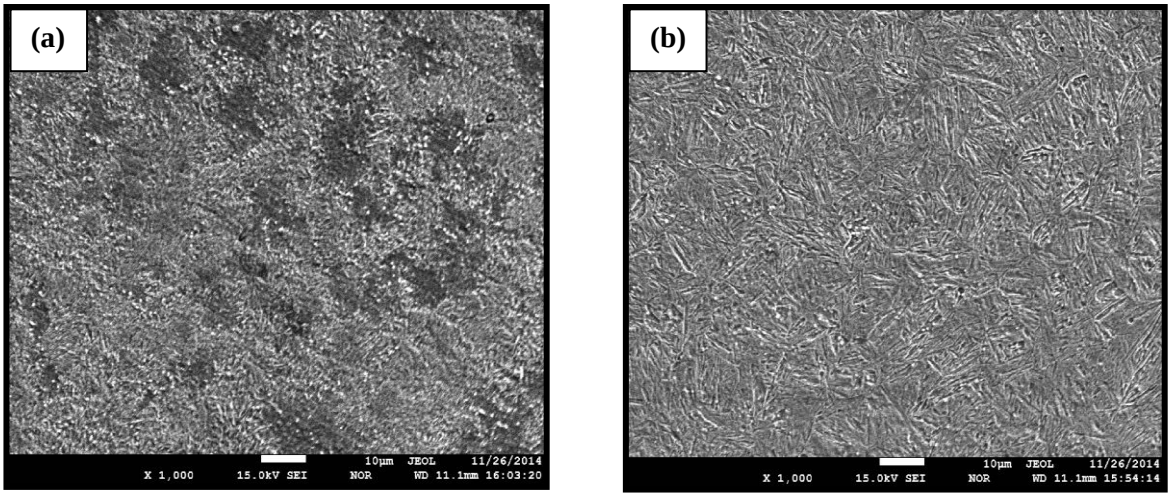

Fig. 4.2: SEM microstructure of (a) annealed (b) normalised samples of AISI 4340 steel at 1000X magnification.

4.3 Study of mechanical properties

4.3.1 Hardness testing

The Vickers hardness test was carried out for the heat treated samples. The hardness values of annealed and normalised specimens are shown in table 4.2. A comparison of the hardness values of annealed and normalised samples indicates that average hardness of the normalised samples was 321 VHN which was higher as compared to the annealed samples with average hardness of 228 VHN. The normalised samples are being subjected to faster cooling rate showed increase in its hardness value. These results are in accordance with a few published reports [38], hence it can be stated that the heat treatment of investigated steel was proper. Further, low standard deviation in hardness values indicates that the values are repetative.

Table 4.2: Vickers hardness values for annealed and normalised samples of AISI 4340 Steel.

Sl. No.	Annealed		Normalised	
	HV_{20}	**Average**	**HV_{20}**	**Average**
Indentation 1	229	228±1.13	323	321±1.17
Indentation 2	226		321	
Indentation 3	229		320	

4.3.2 Tensile test

The tensile properties of the investigated steel in annealed and normalised conditions have been studied using cylindrical samples; the detailed test procedure is mentioned in Section 3.5.2. Typical engineering stress-strain diagrams for the investigated steel for annealed and normalised specimens are illustrated in Fig. 4.3 (a) and (b). Both annealed and normalised specimens showed continuous yielding behavior from elastic to plastic region and hence their yield strength is estimated by 0.2% strain off-set procedure, as suggested in ASTM standard E8M [61]. The tensile properties of the annealed and normalised samples are given in table 4.3. All the values which are tabulated were almost near to standard values of this particular selected steel as mentioned in ASM hand book [38]. Hence it can be stated that the heat treatment and specimen design of investigated steel were proper. The main focus to perform this test is that to calculate stress amplitude and mean stress from the ultimate tensile stress which were used in fatigue test and to compare the properties with standard values of this steel. Estimating the stress values from the above stress strain plots for annealed and normalised specimens and comparing the results, the yield strength and ultimate tensile strength of the annealed specimen were found to be 616 MPa and 906MPa which are less as compared to the normalised specimen which were 1300 MPa and 1467 MPa respectively. This shows that the normalised specimen has more strength

compared to annealed specimen because of finer grain size induced due to air cooling as expected. The uniform elongation (ε_u) of annealed specimen found as 8.86% and for normalised specimen was 4.62%. The total elongation (ε_t) of annealed specimen and normalised specimen was 16.11% and 11.94% respectively. From this it can be concluded that the normalised specimen being stronger and less ductile and less elongation showed as compared to annealed specimen.

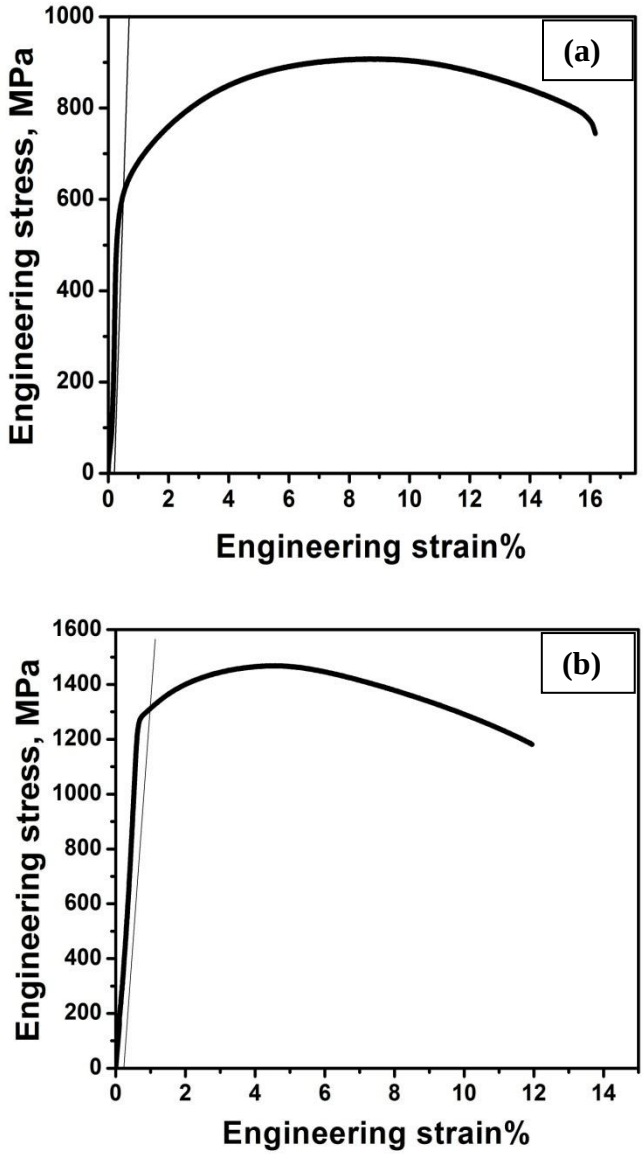

Fig. 4.3: Engineering stress strain curve for (a) annealed and (b) normalised samples of AISI 4340 steel.

The strain hardening exponent (n) of the AISI 4340 steel was estimated by calculating the true stress (σ) and true strain (ε) values from the engineering stress and engineering strain respectively. The log(true stress) vs. log (true strain) plots in the strain range of 1.68 to 4.13 for annealed, 1.11 to 2.88 for normalised samples result into straight lines as shown in Fig. 4.4. The strain hardening exponent values were calculated by using Hollomon equation $\sigma = K\varepsilon^n$, where K is strength coefficient. The values of n are summarized in the table 4.3.

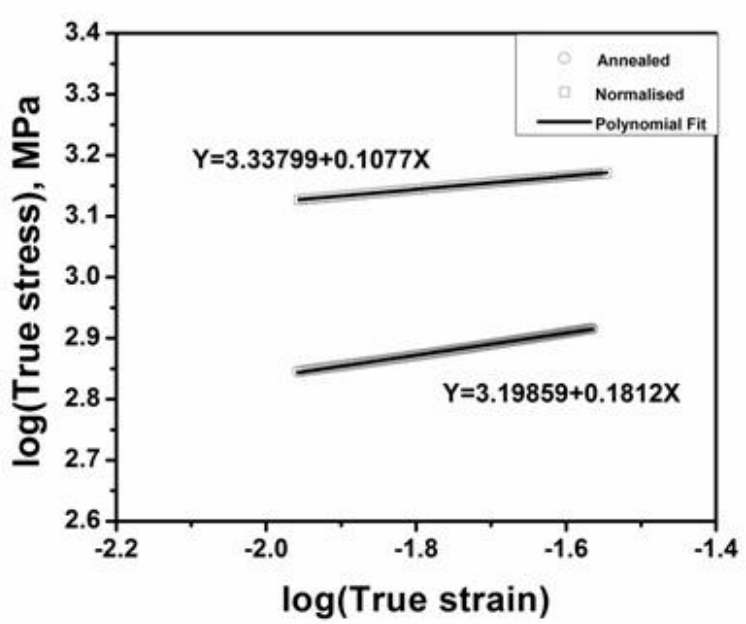

Fig. 4.4: Comparison of the log (σ) – log (ε) plots for annealed and normalised samples of AISI 4340 Steel.

Table 4.3: Tensile properties of annealed and normalised samples of AISI 4340 steel.

Strength	**Annealed**	**Normalised**
Yield Strength (MPa)	616	1300
Ultimate tensile strength (MPa)	906	1467
Strain Hardening Exponent (n)	0.18	0.10
Uniform elongation (ε_u) %	8.86	4.62
Total elongation (ε_t) %	16.11	11.94

4.3.3 Analyses of fatigue tests

4.3.3.1Ratcheting by varying stress ratio:

The results of cyclic tests conducted up to 100 cycles under various stress ratios in annealed and normalised conditions are presented and discussed in this section. Figure 4.5 (a) and (b) show the hysteresis loops of first, 50^{th} and 100^{th} cycles at stress ratio of R = -0.4 for both annealed and normalised specimens respectively. During stress controlled fatigue, the accompanying variation in strain range with progression of cycles is due to the change in hardening or softening response of the material.

Kang et al. [15] explained that the ratcheting strain increases gradually and stress–strain hysteresis loops become wider, if there is cyclic softening feature of the material. As one can visualize that, if the hysteresis loop area increases, a material shows cyclic softening behavior and if the hysteresis loop area decreases there exists cyclic hardening [18-21]. This hardening/softening feature of materials depends greatly on the different heat treatments experienced [18].

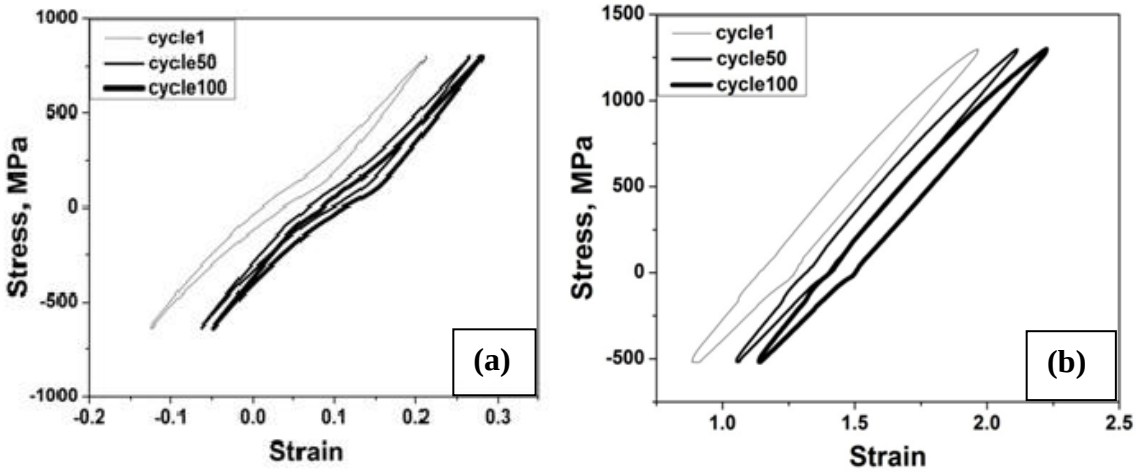

Fig. 4.5: Typical hysteresis loops generated during ratcheting tests at R= -0.4 for (a) annealed (b) normalised specimens.

From Fig. 4.5, it is clear that hysteresis loops shift towards more strain direction during ratcheting deformation, which in turn induces plastic strain to the material. Strain accumulation is calculated by taking the average of minimum and maximum strain in particular cycle. The loop area decreased from first cycle to last cycle i.e., the strain

accumulation is decreased from first cycle to last cycle. This indicates clearly that the selected material shows cyclic hardening behavior.

Yoshida [21] reported that the strain accumulation for R = -0.4 is slightly larger than the R = 0.8, 0.0, -0.8 and -1.0. But the difference in the magnitude of strain accumulation is not so large between stress ratios of others. Kang et al. [15] explained that the most significant ratcheting occurs at the stress ratio of 0.889, even if the increasing stress ratio also results in a weaker ratcheting behavior in 42CrMo steel. Figure 4.6 (a) and (b) depict the variations in ratcheting strain with number of cycles at different stress ratios in both annealed and normalised conditions. As the stress ratio increases ratcheting strain also increases in both annealed and normalised samples and the magnitude of strain accumulation in ratcheting of R = -0.4 is slightly higher than that in case of R= -0.6 and -0.8. Larger strain accumulation at a given number of stress cycles is found at stress rate of R=-0.4.All these details summarized in table 4.4. These features are partially similar to those obtained by Yoshida [21], for SUS304 stainless steel but totally different from 42CrMo steel [15]. This fact causes increased amount of dislocation generation when stress ratio is increased to higher level. The increase in strain accumulation with increasing stress ratio can be described as a consequence of increasing dislocation density, at higher stress ratio levels [72].

Table 4.4: Ratcheting strain variation with respect to stress ratio.

S. No.	**Stress ratio (R)**	**Ratcheting strain %**	
		Annealed	**Normalised**
1	-0.4	1.16	1.0
2	-0.6	0.62	0.94
3	-0.8	0.40	0.81

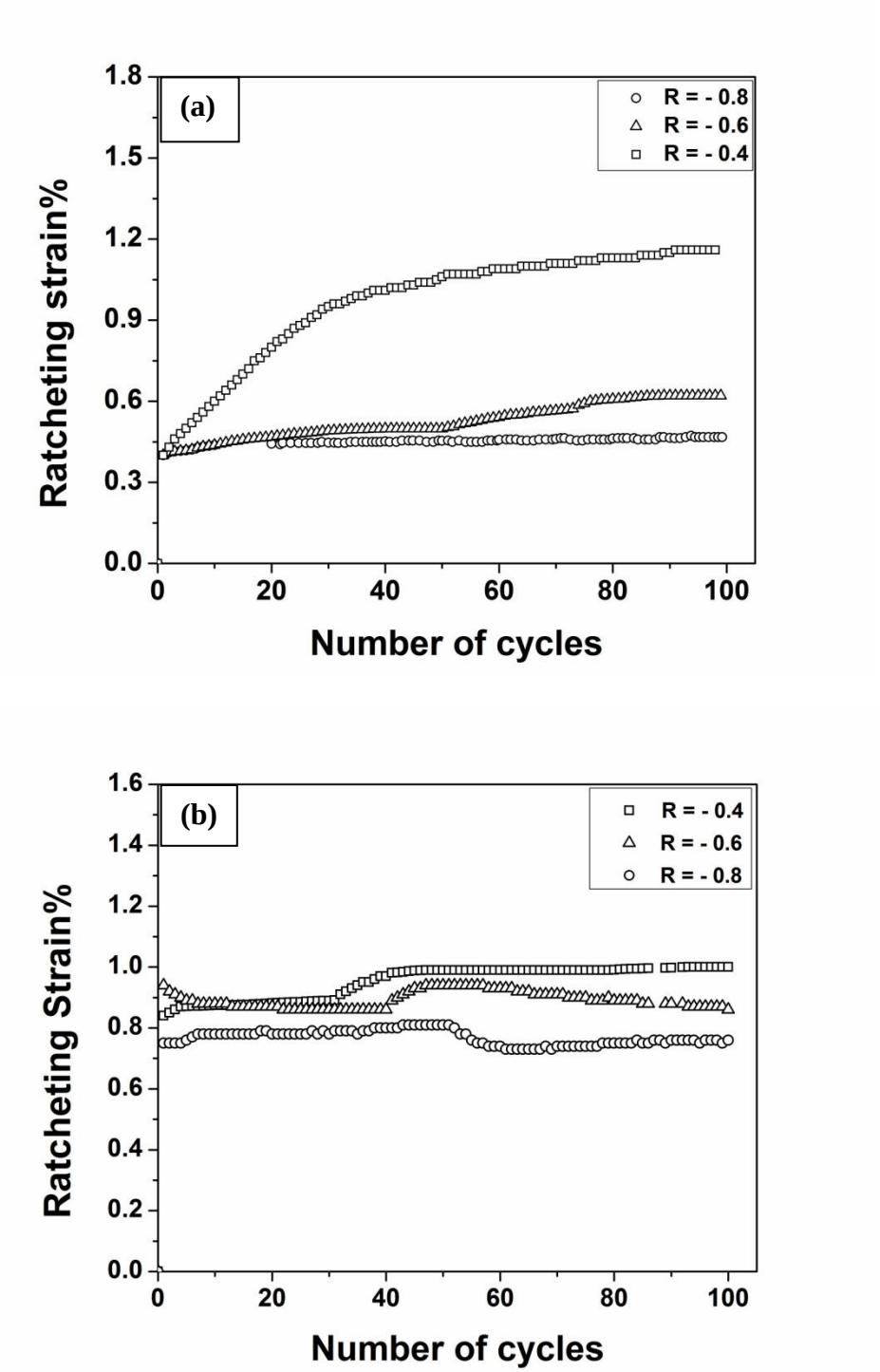

Fig. 4.6: Effect of stress ratio on ratcheting strain at R= -0.4, -0.6 and -0.8 in (a) annealed (b) normalised specimens.

Xia et al. [13] observed that the rate of accumulation of ratcheting strain i.e., the increment of ratcheting strain in each cycle decreases gradually with the number of cycles due to its cyclic hardening feature in ASTM A-516 Gr.70 steel. Chen et al. [8] observed that the ratcheting strain increases in high-nitrogen steel X13CrMnMoN18-14-3 whereas its rate decreases continuously with increasing number of cycles. Dutta and Ray [23] observed that rapid accumulation of ratcheting strain in the initial few cycles followed by attainment of a steady state value in ratcheting rate are the characteristic features of the asymmetric cyclic deformation behavior of IF steel. All these studies indicate that strain accumulation takes a saturation plateau after few cycles of loading. In this study also, the nature of attainment of steady state has been examined. Figure 4.7 (a) and (b) depict the variations in ratcheting strain rate effect with number of cycles at different stress ratios in both annealed and normalised conditions respectively. From Fig.4.7, it can be seen that the rate of strain accumulation decreases continuously up to initial few cycles after that it reaches saturation level in both annealed and normalised conditions. It can also be stated that there is no much variation in ratcheting strain rate at different stress ratios.

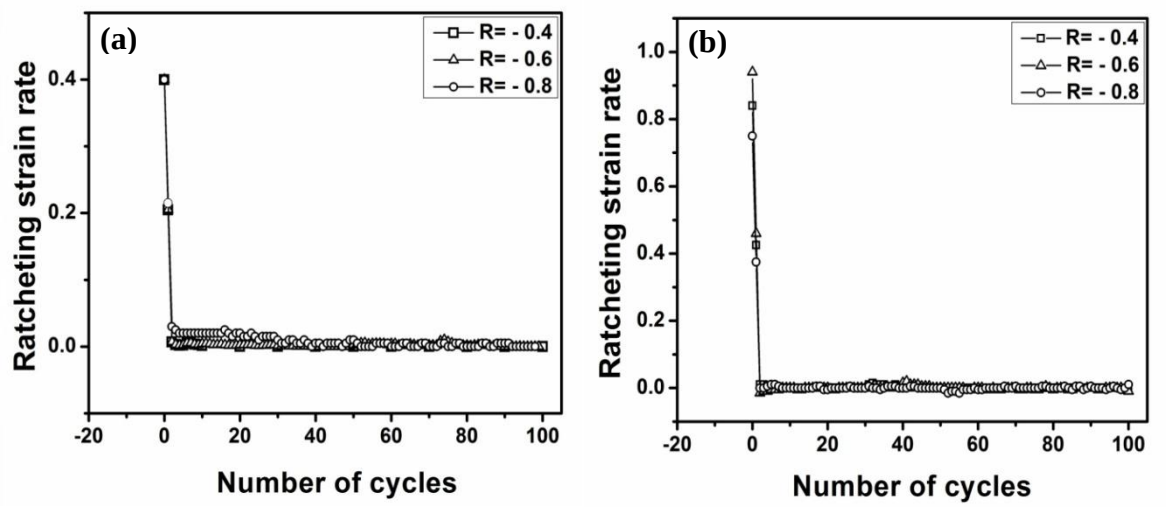

Fig. 4.7: Variation in the rate of accumulation of ratcheting strain with increasing number of cycles for (a) annealed (b) normalised AISI 4340 steel at different stress ratio.

4.3.3.2 Effect of previous ratcheting deformation on low cycle fatigue behavior of the steel

It is known that ratcheting deformation causes plastic damage to a material and thus, it affects the properties of the material. To see the effect of previous ratcheting on the low cycle fatigue behavior of the investigated material, one set of samples were tested for strain controlled low cycle fatigue tests and another set of samples were first ratcheted upto 100 cycles followed by strain controlled low cycle fatigue tests; both types of results are compared in terms of stress amplitude. The LCF tests were carried out at strain amplitudes of ±0.50 and ±0.75 whereas the ratcheting tests done at stress ratio of -0.4.

In strain controlled fatigue cyclic hardening and softening would lead to increasing and decreasing peak stress with increasing cycles respectively [1]. Figure 4.8 (a) and (b) represents the hysteresis loops of 1^{st}, $50^{th}$and 100^{th} cycles which were produced during strain controlled tests for the annealed AISI 4340 steel at strain amplitudes of ±0.50 and ±0.75 respectively. The loop heights increase from 1^{st} cycle to last cycle that means the material showing hardening behavior. The hysteresis loop area at strain amplitudes of ±0.50 and ±0.75 are tabulated in table 4.5. These results are similar to those obtained by Zhu et al. [66] for Mg–10Gd–2Y–0.5Zr alloys and totally different from that of carbon steel 45 [32], Cr-Mo-V high speed steel [66], 34CrMoNi steel [67]. From this experiment it can be concluded that in both stress controlled and strain controlled tests, the material showed hardening behavior.

Paul et al. [27] reported that with increasing applied strain amplitude, the degree of cyclic hardening initially increases and saturates at higher strain amplitude. Figures 4.9 (a) and (b) displays the stress amplitude vs. number of cycles relationship for only LCF and post ratcheting LCF respectively.

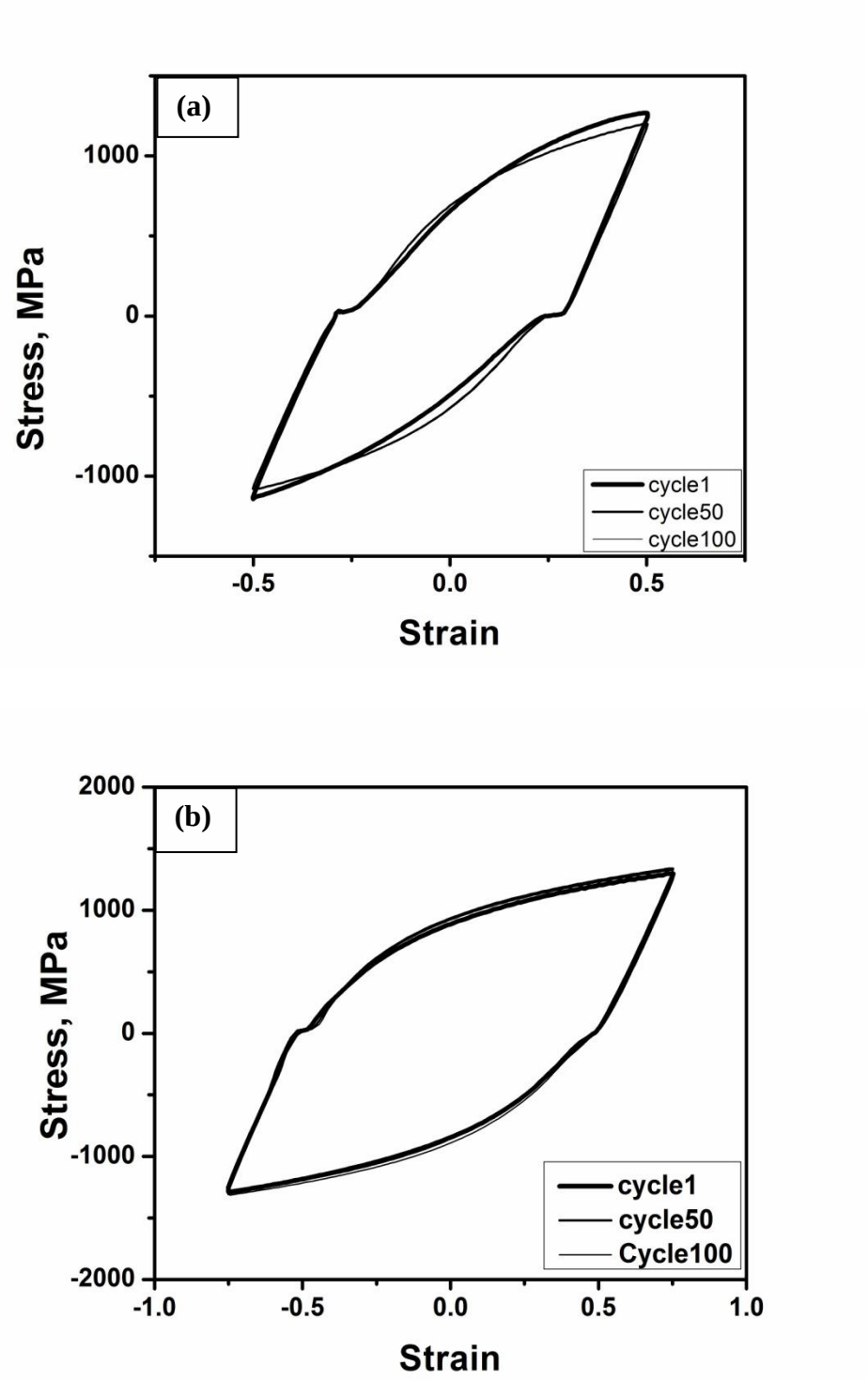

Fig. 4.8: Hysteresis loops produced during strain controlled LCF tests at strain amplitudes of (a) ±0.50 (b) ±0.75 of annealed AISI 4340 steel.

Table 4.5: Hysteresis loop area at strain amplitudes ±0.50 and ±0.75 for annealed AISI 4340 steel.

Strain amplitude	Hysteresis loop area (MJ/m^3)
±0.50	850
	880
	885
±0.75	1881
	1912
	1935

It is noted from Fig 4.9 (a) and (b) that for annealed AISI 4340 steel, the stress amplitudes in the cyclic straining with different applied strain amplitudes are different. The stress amplitude obtained as 1217 MPa and 1323 MPa at strain amplitudes of ±0.50 and ±0.75 respectively. At higher levels of cyclic straining (i.e., at ±0.75), hardening is rapid in the first few cycles, followed by an almost steady but low rate of hardening. It may be noted that complete saturated state of hardening is not exhibited. Similar dependency of cyclic hardening on imposed strain amplitude was also reported for austenitic stainless steels, such as AISI 304L and AISI 316 [69–72]. For another set of samples ratcheting tests were done up to 100 cycles and again LCF tests (LCF followed by ratcheting) conducted on same samples at same conditions. The stress amplitude obtained in LCF after ratcheting as 1363 MPa and 1426 MPa at same strain amplitudes. All these details mentioned in table 4.6.The results indicate that almost 10% increment in peak stress takes place for the lower strain amplitude test while the increment in peak stress is 7% for higher strain amplitude. By this experimental results it is concluded that the stress amplitudes were increased at both strain amplitudes after ratcheting followed by LCF test compared to only LCF tests. The fact of increased stress amplitude in ratcheting plus LCF specimens can be attributed to the previous cyclic hardening during ratcheting tests.

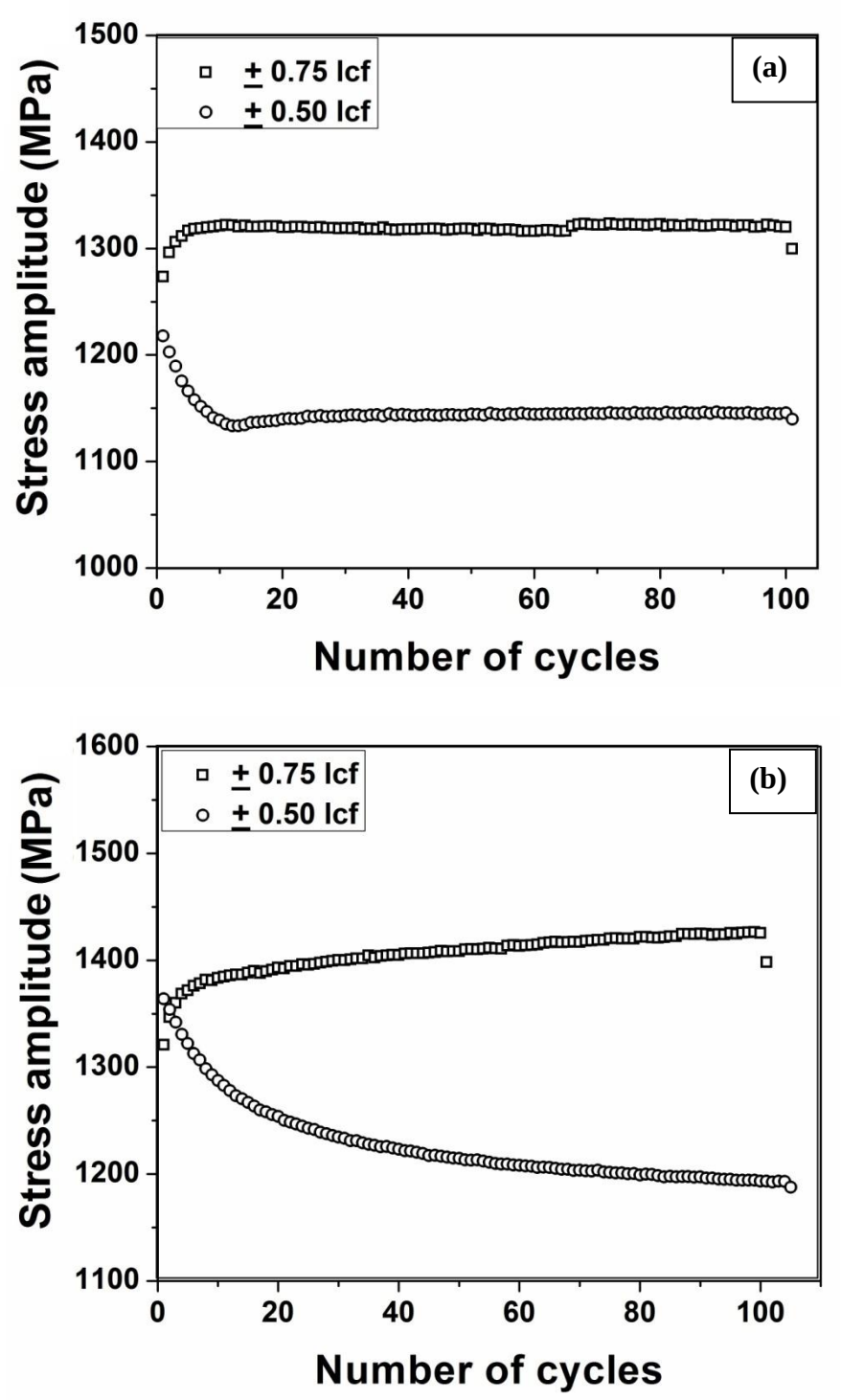

Fig. 4.9: Stress amplitude values at strain amplitudes of ±0.50 and ±0.75 in a) only LCF b) after ratcheting LCF.

Table 4.6: Stress amplitude values after LCF test at strain amplitudes ±0.50 and ±0.75.

S. No.	Test parameter	Strain amplitude	Stress amplitude (MPa)
1	Only LCF	±0.50	1217
		±0.75	1323
2	After ratcheting LCF	±0.50	1363
		±0.75	1426

4.3.3.3 Effect of previous low cycle fatigue deformation on ratcheting behavior of the steel

To see the effect of previous low cycle fatigue deformation on the ratcheting behavior of the investigated material, one set of samples were tested for ratcheting and for another set of samples first tested for LCF up to 100 cycles and that was followed by ratcheting tests; both types of results are compared in terms of accumulated ratcheting strain. The LCF tests were carried out at strain amplitudes of ±0.50, ±0.75 and the ratcheting tests done at stress ratio of -0.4. Figure 4.10 (a) and (b) illustrate the comparison between only ratcheting and after LCF plus ratcheting. The sample which was tested for only ratcheting showed a strain accumulation of 9.4%. On the other hand, the samples which were previously fatigue loaded, showed varying strain accumulations of 7.5% and 4.8 % for strain amplitudes of ±0.50 and ±0.75. All these details are mentioned in table 4.7. A decrease of ratcheting strain observed in ratcheting after LCF test. The results indicate that ratcheting strain rapidly increased up to first few cycles, then it was gone towards saturation by slow increase of strain up to 20 cycles after that saturation in strain accumulation is achieved.

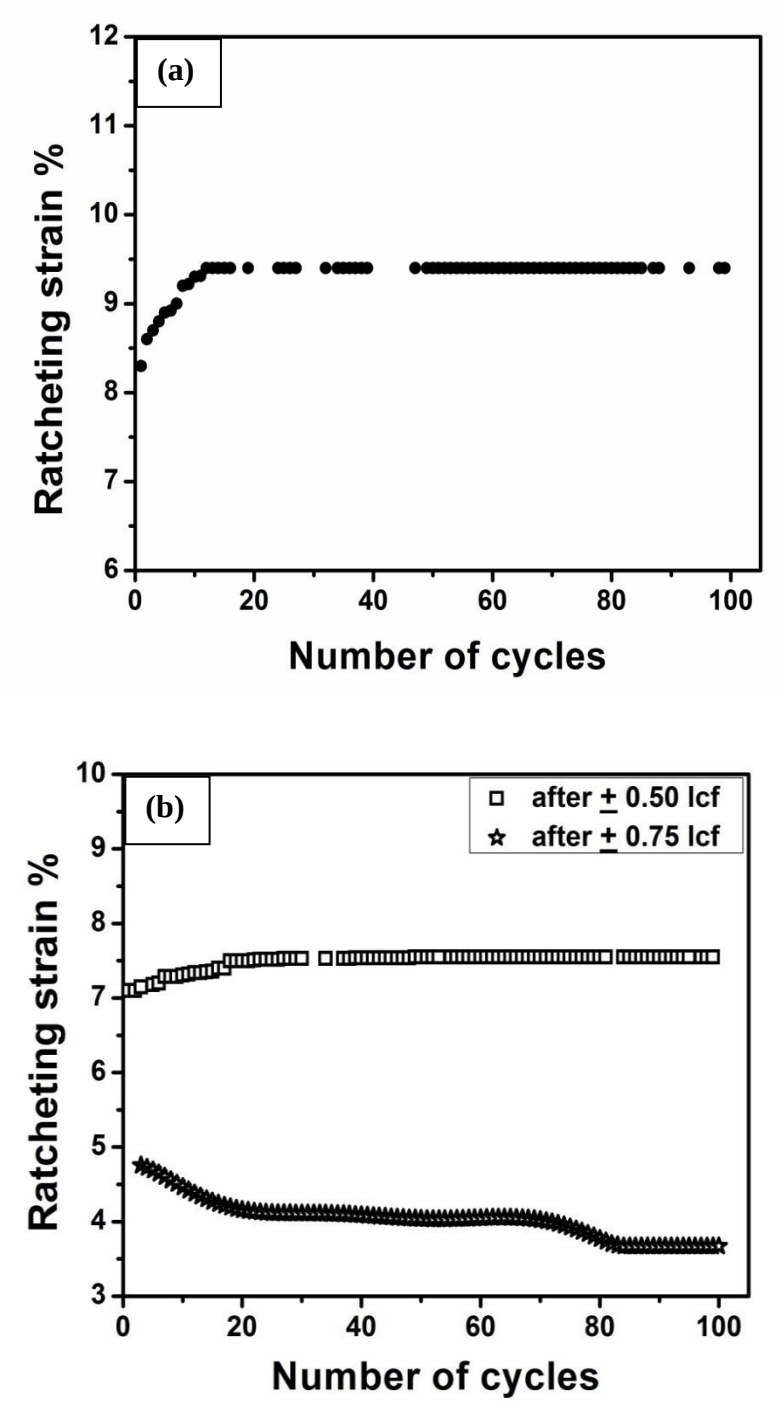

Fig. 4.10: Ratcheting strain at stress ratio of -0.4 in a) only ratcheting b) after LCF ratcheting.

Table 4.7: Ratcheting strain values after ratcheting test at stress ratio R = -0.4.

S. No.	Test parameter	Stress ratio	Ratcheting strain%
1	Only ratcheting	R= -0.4	9.4
2	After LCF ratcheting	After ±0.50 LCF at R=-0.4	7.5
		After ±0.75 LCF at R= -0.4	4.8

4.4 Post ratcheting tensile

To understand the effect of previous strain accumulation on tensile properties of ratcheted specimens; tensile tests were carried out on a series of specimens after 100 cycles of ratcheting, subjected to varying stress ratio conditions. Mahato et al. [71] observed that post ratcheting yield and ultimate tensile strength of copper increased as compared to unratcheted samples and these are decreased with decreasing stress ratio. Dutta et al. [23, 72] reported that both yield strength and ultimate tensile strength of IF steel and Aluminum alloy increase as compared to unratcheted values. Figure 4.11 (a) and (b) show the post ratcheting tensile plots for both the heat treated conditions. All the details related to these tests are summarized in table 4.8.The results clearly showed that yield strength and ultimate tensile strength increased as also shown in Fig.4.11. Further, the results indicate that the strength values are higher at stress ratio R= -0.4 than at R= -0.6 and -0.8 in both annealed and normalised samples. The strain hardening exponent values for post ratcheted tensile samples increased compared to unratcheted one in both annealed and normalised conditions. This fact indicates that the strength of the ratcheted steel is governed by increased strain hardening [23]. From the results it can be concluded that post ratcheting yield strength and ultimate tensile strength of selected steel increased as compared to unratcheted samples and these are decreased with decreasing stress ratio.

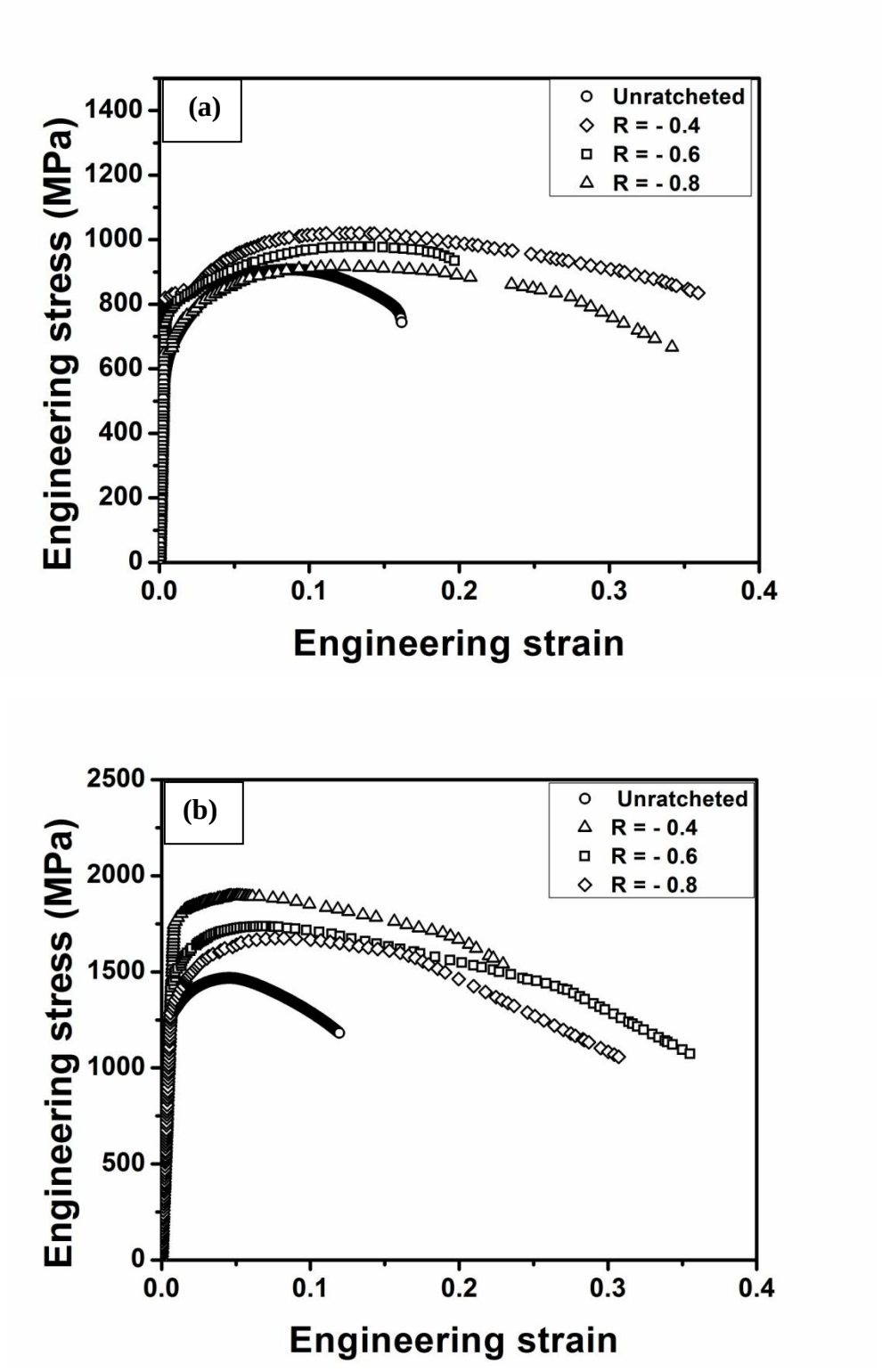

Fig. 4.11: Post ratcheting tensile stress-strain plots for (a) annealed and (b) normalised samples of investigated steel.

Table 4.8: Post ratcheting tensile test values for annealed and normalised samples at different stress ratios.

Properties	Stress ratio	Yield strength (MPa)	Ultimate tensile strength (MPa)	Strain hardening exponent (n)
Annealed	Unratcheted	616	906	0.18
	R= -0.4	854	1019	0.18
	R= -0.6	833	978	0.17
	R= -0.8	769	916	0.15
Normalised	Unratcheted	1300	1467	0.10
	R= -0.4	1380	1895	0.10
	R= -0.6	1621	1737	0.11
	R= -0.8	1504	1675	0.13

4.5 Post ratcheting hardness

To assess the extent of deformation during cyclic loading, post-ratcheting hardness tests were also carried out on ratcheted samples. In order to do this, Vickers hardness tests were done on a series of specimens cut from the guage portions of post ratcheting tensile samples after post-ratcheting tests; the results are listed in table 4.9. It can be noticed that hardness values of the investigated steel specimens increased after ratcheting deformation. Bhattacharyya et al. [73], reported similar increase in hardness of specimens subjected to their rolling cycle fatigue. They have reported that increase in hardness can be a result of cyclic hardening, which takes place due to continuous plastic strain accumulation. Hence in this investigation increase in hardness can be considered due to the effect of strain hardening due to ratcheting deformation. It is clear from the table 4.9 that hardness varies with stress ratio i.e., as the stress ratio decreases, hardness decreases. Hence from the results it can be concluded that at more negative stress ratio, the hardness increases in the investigated steel.

Table.4.9: Post ratcheting hardness values for annealed and normalised samples at different stress ratios.

Stress ratio	Annealed		Normalised	
	HV_{20}	**Average**	**HV_{20}**	**Average**
Unratcheted	229	228±1.13	323	321±1.17
	226		321	
	228		320	
-0.4	329	331±1.94	462	462±2.30
	330		463	
	333		459	
-0.6	3 01	302±1.86	447	444±2.40
	304		442	
	302		443	
-0.8	252	253±1.68	427	424±2.75
	253		424	
	255		421	

4.6 Fractographic Observation

The fracture surfaces of broken tensile samples which were previously ratcheted as well low cycle fatigued were examined by means of scanning electron microscope (SEM) using the secondary electron signal. Figure 4.12 show the SEM images of the fracture surfaces of post ratcheted tensile samples at different of low cycle fatigue and ratcheting conditions. The fractographs reveal ductile morphology with greater number of dimples as shown in Fig. 4.12 although all the specimens are having distinct signatures of precious cyclic loading on their morphologies. So, the fracture surfaces in Fig. 4.12 confirm with the induced ductility in the ratcheted and low cycle fatigue annealed samples.

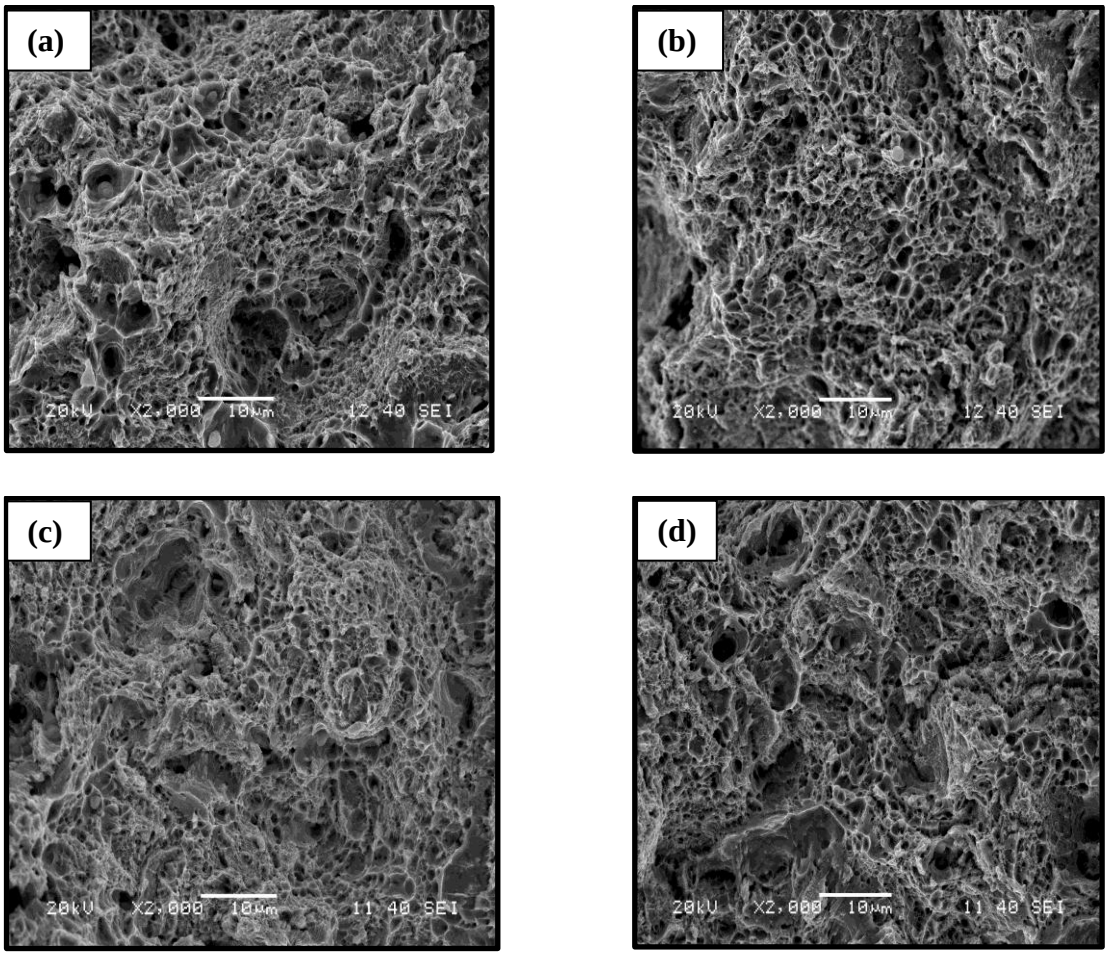

Fig. 4.12: Typical fractographs (a) Ratcheting and LCF at ±0.50 (b) Ratcheting and LCF at ±0.75 (c) LCF at ±0.50 and ratcheting (d) LCF at ±0.75 and ratcheting.

Elemental analyses of inclusions were done using energy dispersive spectroscopy (EDS). Figure 4.14 shows the EDS spectra of Ratcheting plus LCF and LCF plus ratcheting at strain amplitude of ±0.50 samples respectively. The results show that mainly Fe-based inclusions are present in the investigated AISI 4340 steel. It is reported that the inclusions in investigated steel can be Fe_3P, $Fe_2Si_2Al_9$ or a mixture of the two. MnS type inclusions also can be expected in this type alloy.

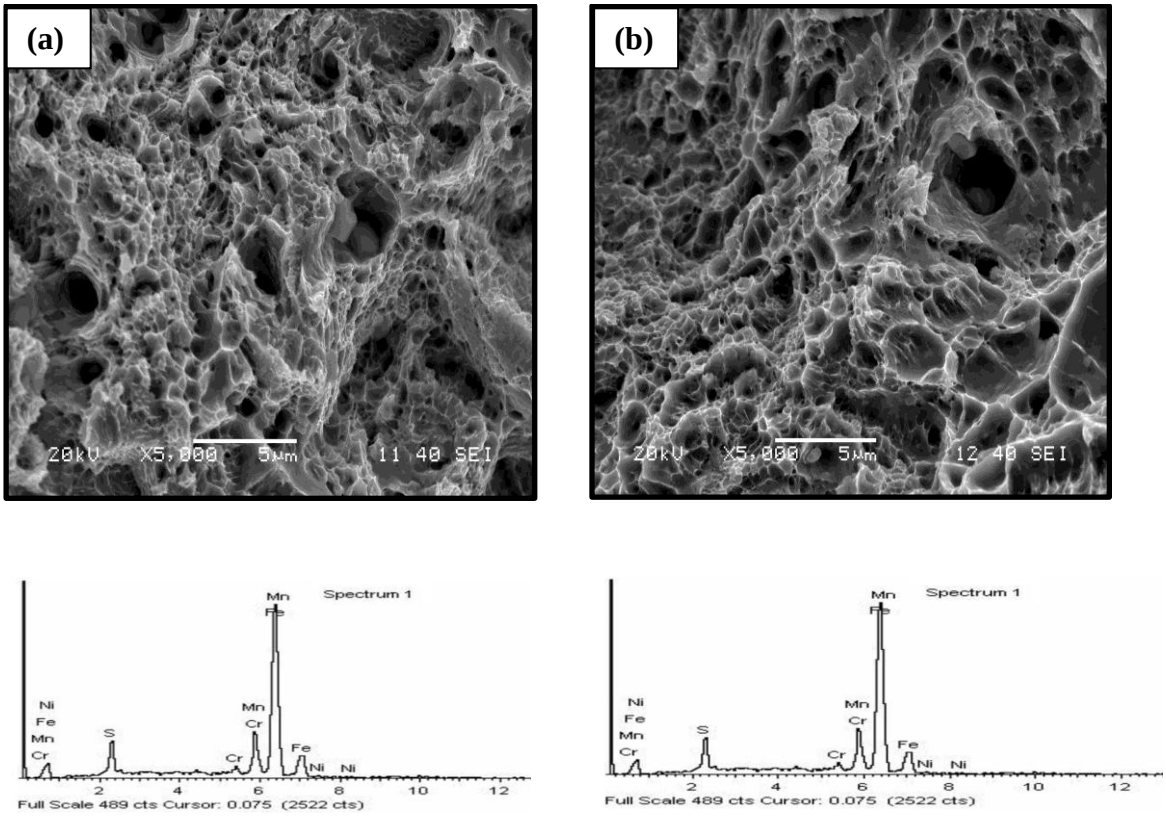

Fig. 4.13: EDS spectra of (a) Ratcheted plus LCF (b) LCF plus ratcheted samples at strain amplitude of ±0.50 of AISI 4340 steel.

4.7 XRD profile analysis

A series of X-ray diffraction experiments were done for all the fatigue specimens of the investigated AISI 4340 steel after 100 cycles of both ratcheting and strain controlled tests on transverse section of the gauge portion. This test carried out to understand the extent of deformation on the investigated steel. The patterns were examined by comparing the positions and intensities of samples with those in the (JCPDS) data files. Figure 4.14 shows the X-ray diffraction patterns of the investigated material which consists of α-iron peaks and its (*hkl*) values at different loaded conditions. The X-ray diffraction profiles used for the analysis were (110), (200), (211), and (220) corresponding to α-Fe (bcc) phase.

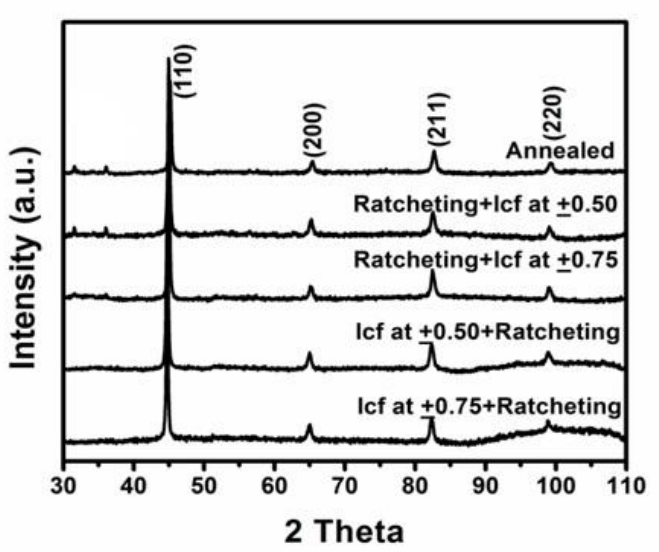

Fig. 4.14: X-ray diffraction patterns of the different fatigue loaded samples of investigated steel.

Ungar et al. [77, 78] reported that dislocation density of different materials can be calculated by analyzing the full width half maximum of the corresponding XRD peaks. For this modified Williamson Hall equation can be used which can be written as:

$$\Delta K \cong 1/d + \frac{\pi M^2 b^2}{2} \rho^{1/2} \left(K^2 \overline{C}\right) + O\left(K^4 \overline{C}^2\right)$$

Where, K = 2 sin θ/λ and ΔK = 2 cos θ Δθ/λ and θ, Δθ are the diffraction angle and the integral breadth of the diffraction peak. $\bar{C}$ represents the average contrast factor of the dislocations for a particular reflection and this is related to material's elastic constant [77]. M is a constant depending on both the effective outer cut-off radius of dislocations and the dislocation density. The value of M varies in between1 and 2 for deformed materials [77-80]. In this investigation the value of M considered 2. The ΔK for each (*hkl*) peak is plotted as a function of $K\bar{C}^{1/2}$ as shown in Fig.4.15 and the slope (m) of the fitted curve is used to calculate the dislocation density from the following equation,

$$\rho = \left[\frac{2m^2}{\pi M^2 b^2}\right]$$

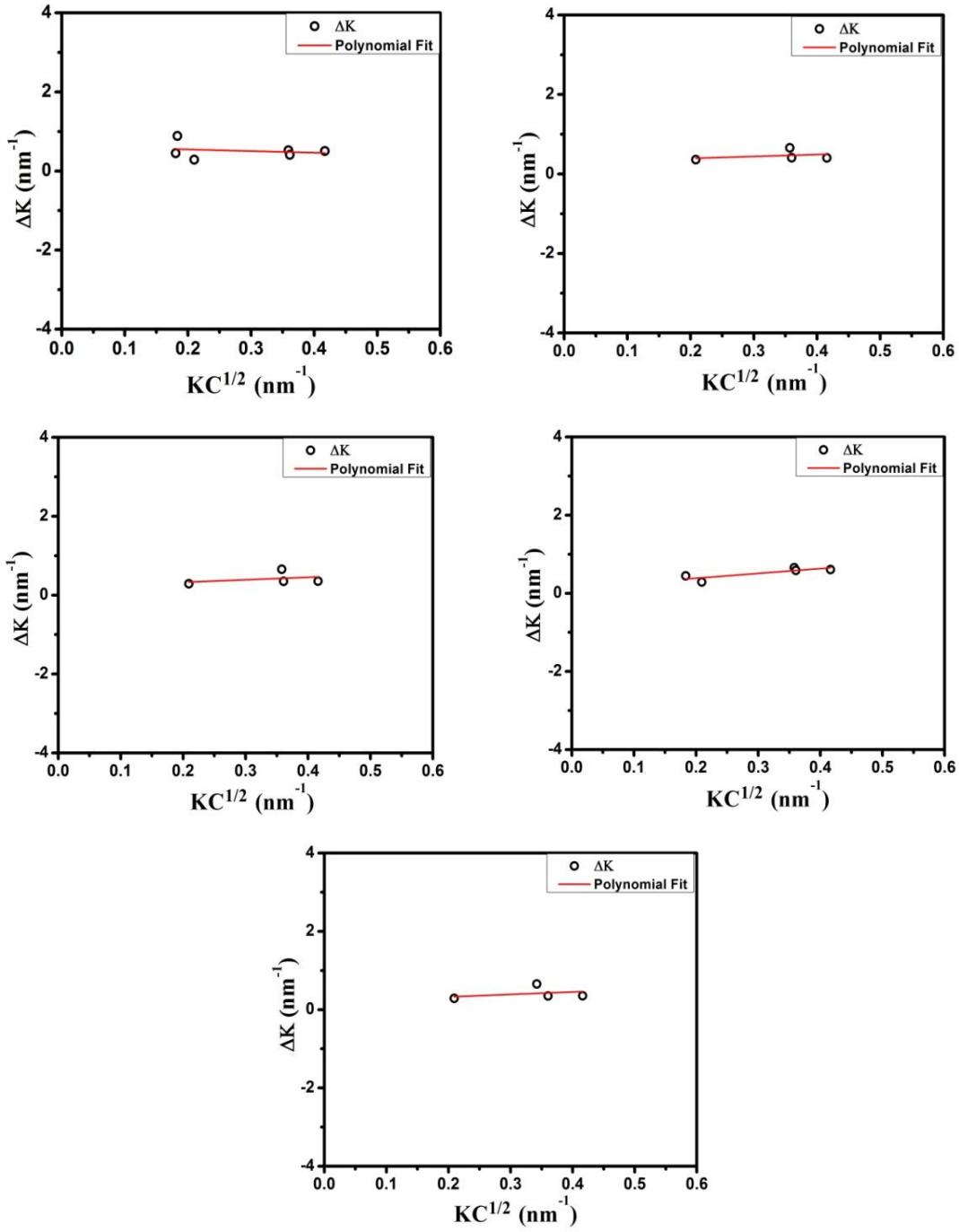

Fig. 4.15: ΔK verses $K\bar{C}^{1/2}$ plots for (a) annealed (b) LCF at ±0.50 plus ratcheting (c) LCF at ±0.75 plus ratcheting (d) Ratcheting plus LCF at ±0.50 (e) Ratcheting plus LCF at ±0.75.

The obtained dislocation density values for undeformed and low cycle fatigue loaded samples are tabulated in the table 4.10. One can note that dislocation density increased after ratcheting deformation as well low cycle fatigue. Few researchers also discussed in their recent reports that strain accumulation due to ratcheting depends on dislocation formation and their redistribution [80-81].

Table 4.10: Dislocation density variation between deformed and undeformed samples of investigated steel.

Stress condition		**Dislocation density (m^{-2})**
Undeformed	-	6.65×10^{8}
Ratcheting + LCF at ±0.50	Stress amplitude of 1363 MPa	1.59×10^{18}
Ratcheting + LCF at ±0.75	Stress amplitude of 1426 MPa	1.18×10^{19}
LCF at ±0.50 + Ratcheting	Ratcheting strain of 7.5%	1.58×10^{18}
LCF at ±0.75 + Ratcheting	Ratcheting strain of 4.8%	9.09×10^{17}

CHAPTER 5

CONCLUSIONS AND SCOPE FOR FUTURE WORK

CONCLUSIONS AND SCOPE FOR FUTURE WORK

5.1 Conclusions

The obtained results and their pertinent analyses related to fatigue-ratcheting interaction behavior of AISI 4340 steel at room temperature assist to infer:

1. Accumulation of ratcheting strain increased with increasing stress ratio in both annealed and normalised samples of AISI 4340 steel. Maximum accumulation of ratcheting strain (1.16% for annealed and 1.02% for normalised) was observed at R = -0.4 up to the investigated number of cycles. Rate of strain accumulation is decreased from first cycle to last cycle. This indicates clearly that the selected material shows cyclic hardening behavior. The increase in strain accumulation can be explained with increased dislocation densities in the ratcheted samples.
2. Prior strain controlled low cycle fatigue (LCF) deformation reduces the accumulation of ratcheting strain in the investigated steel, in comparison to that in only ratcheted specimens. On the other hand, when the samples were ratcheted prior to strain controlled LCF tests, the required stress amplitudes increase to deform the specimen, as compared to only LCF tests. The samples which were previously fatigue loaded, showed increase in stress amplitude and decrease in strain accumulation due to cyclic hardening behavior of material.
3. Post ratcheting yield strength, tensile strength and hardness of investigated steel increased as compared to unratcheted samples and these increased with increasing stress ratio. The fact can be attributed to the previous cyclic hardening during ratcheting tests. The fractographic features also carries this signature.
4. XRD of previously fatigued samples evidenced the increased dislocation density values, as that compared with the undeformed specimens.

5.2 Scope for future work

1. In the present investigation fatigue-ratcheting interaction behavior of AISI 4340 steel has been studied in annealed and normalised conditions. However, there is enough scope to study the behavior in other heat treated conditions.
2. To study the dislocation sub-structure formation, TEM analysis could be done.
3. Simulation of the ratcheting behavior of this material at different heat treated conditions may also be the future work.

CHAPTER 6

REFERENCES

References

1. G.E., Dieter, Mechanical metallurgy, McGraw Hill Ltd., UK, 1988, pp 375, 376, 378, 390.
2. G. Kang, Q. Gao, X.J. Yang, Mechanical Materials, 34 (2002) 145–159.
3. K. Dutta, S. Sivaprasad, S. Tarafder, K.K. Ray, Materials Science and Engineering A 527 (2010) 7571–7579.
4. X. Chen, D.H. Yu, K.S. Kim, Materials Science and Engineering A 406 (2005) 86–94.
5. R. Kreethi, P. Verma, K. Dutta, Transaction of the Indian Institute of Metals, 68 (2015) 229–237.
6. P. Zhao, F.Z. Xuan, Mechanical Materials, 43 (2011) 299–312.
7. C.B. Lim, K.S. Kim, J.B. Seong, International Journal of Fatigue 31 (2009) 501–507.
8. G. Chen, S.C. Shan, X. Chen, H. Yuan, Computational Materials Science 46 (2009) 572–578.
9. A. Sarkar, A. Nagesha, R. Sandhya, M.D. Mathew, Procedia Engineering 55 (2013) 650–654.
10. Y. Wang, D. Yu, G. Chen, X. Chen, International Journal of Fatigue 52 (2013) 106–113.
11. A.V. Farahani, Theoretical and Applied Fracture Mechanics 73 (2014) 152–160.
12. S. Vishnuvardhan, G. Raghava, P. Gandhi, M. Saravanan, D.M. Pukazhendhi, S. Goyal, P. Arora, S.K. Gupta, Procedia Engineering 2 (2010) 2209–2218.
13. Z. Xia, D. Kujawski and F. Ellyin, International Journal of Fatigue 18 (1996) 335–341.
14. S. Kwofie, International Journal of Fatigue 23 (2001) 829–836.
15. G. Kang, Q. Gao, X. Yang, Mechanical Materials 34 (2002) 521–531
16. X.M. Chen, Y.C. Lin, J. Chen, Journal of Alloys and Compounds 579 (2013) 540–548.
17. X. Chen, R. Jiao, K.S. Kim, International Journal of Plastics 21 (2005) 161–184
18. G. Kang, Y. Liu, Z. Li, Material Science and Engineering A 435–436 (2006) 396–404.
19. G.Z. Kang, Y.G. Li, J. Zhang, Y.F. Sun, Q. Zao, Theoretical and Applied Fracture Mechanics 43 (2005) 199–209.
20. Y. Liu, G. Kang, Q. Gao, International Journal of Fatigue 30 (2008) 1065–1073.
21. F. Yoshida, International Journal of Pressure Vessels and Piping 44 (1990) 207–223.
22. K. K. Ray, K. Dutta, S. Sivaprasad, S. Tarafder, Procedia Engineering 2 (2010) 1805–1813.

23. K. Dutta, K.K. Ray, Materials Science and Engineering A 575 (2013) 127–135.
24. C.H. Lee, V. N.V. Do, K.H. Chang, International Journal of Plasticity 62 (2014) 17–33.
25. Y.C. Lin, X.M. Chena, G. Chen, Journal of Alloys and Compounds 509 (2011) 6838–6843.
26. Y.C. Lin, Z.H. Liu, X.M. Chen, J. Chen, Materials Science and Engineering A 573 (2013) 234–244.
27. S.K. Paul, S. Sivaprasad, S. Dhar, S. Tarafder, Journal of Nuclear Materials 401 (2010) 17–24
28. M. Wen, H. Li, D. Yu, G. Chen, X. Chen, Materials and Design 46 (2013) 426–434.
29. A. Sarkar, P.S. De, J.K. Mahato, A. Kundu, P. C. Chakraborti, Procedia Engineering 74 (2014) 376–383.
30. C.L. Pun, Q. Kan, P.J. Mutton, G. Kang, W. Yan, International Journal of Fatigue 66 (2014) 138–154.
31. X. Yang, International Journal of Fatigue 27 (2005) 1124–1132.
32. G. Kang, Y. Liu, J. Ding, Q. Gao, International Journal of Plasticity 25 (2009) 838–860.
33. H. Cheng, G. Chen, Z. Zhang, X. Chen, Journal of Nuclear Materials 458 (2015) 129–137.
34. X. Chen, S. Hui, Polymer Testing 24 (2005) 829–833.
35. G. Tao, Z. Xia, Polymer Testing 26 (2007) 451–460.
36. G. Tao, Z. Xia, International Journal of Fatigue 29 (2007) 2180–2190.
37. M. Shariati, H. Hatami, H. Yarahmadi, H.R. Eipakchi, Materials and Design 34 (2012) 302–312.
38. ASM Handbook volume 1 properties and selection irons steels and high permance alloys (1990) 1124–1131.
39. Y. Xiong, Q. Yu , Y. Jiang, International Journal of Plasticity 53 (2014) 107–124.
40. G. Kang, Y. Liu, Material Science and Engineering A, 472 (2008) 258–268.
41. R.J. Rider, S.J. Harvey and H.D. Chandler, International Journal of Fatigue 17 (1995) 507–511.
42. Avner, Introduction to physical metallurgy, Tata McGraw-Hill Education, 1997
43. V. Raghavan, Physical Metallurgy: Principles and Practice PHI Learning Pvt. Ltd., 2006.
44. P. Yang, X. Liao, J. Zhu, H. Zhou, International Journal of Fatigue 16 (1994) 327–330.
45. S.K. Chandra, V. Shankar, K. Mariyappan, R. Sandhya, P.C. Chakraborty, Procedia Engineering 55 (2013) 176–180.
46. S.M Lee and Stone Scripta, Metallurgical Materials 23 (1994) 701–707.

47. C. Kanchanomai, Y. Miyashita, Y. Mutoh, International Journal of Fatigue 24 (2002) 987–993.
48. Y. Rong, C. Xiang, R. Hui, Q. Yuan, Journal of Iron and Steel Research, International 20 (2013) 50–56.
49. O. Fatoba, R. Akid, Procedia Engineering 74 (2014) 279–286.
50. H. Hao, D. Ye, C. Chen, Materials Science and Engineering A 605 (2014) 151–159.
51. S. Begum, D.L. Chen, S. Xu, A.A. Luo, Materials Science and Engineering A 517 (2009) 334–343.
52. S.Q. Wang, J.H. Liu, Z.X. Lu, D.L. Chen, Materials Science and Engineering A 598 (2014) 122–134.
53. G. Chai, P. Liu, N. Zhou, J. Frodigh, Procedia Engineering 55 (2013) 671– 676.
54. G. Grzgorz, S. Mrozinski, Engineering Failure Analysis 35 (2013) 692–702.
55. B. Zettle, H. Mayer, C. Ede, S.S. Tschegg, International Journal of Fatigue 28 (2006) 1583–1589.
56. V.S. Srinivasan, R. Sandhya, K. B.S.Rao, S.L. Mannan, K.S. Raghavan, International Journal of Fatigue 13 (1991) 471–478.
57. B.K. Kim, D. Kim, I. Choi, W.S. Jung, S.I. Kwun, Materials Science and Engineering A 577 (2013) 81–86.
58. G. Chen, X. Chen, C.D. Niu, Materials Science and Engineering A 421 (2006) 238–244.
59. S. Shivaprasad, S.K. Paul, S.K. Gupta, V. Bhasin, N. Narasaiah, S. Tarafdar, International Journal of Pressure Vessels and Piping 87 (2010) 464–469.
60. T. Hassan, S. Kyriakides, International Journal Plasticity 10 (1994) 149–184.
61. E 8M-03, 'Annual Book of ASTM Standards', Standard test method for tension testing of metallic materials (Metric), 03.01; 2003, West Conshohocken, PA.
62. E606 / E606M-12, Standard Test Method for Strain-Controlled Fatigue Testing, ASTM International, 2012 West Conshohocken, PA.
63. E112, 'annual book of ASTM standards', standard test methods for determining grain size, 2003, west conshohocken, pa. ASM Handbook volume 8 Mechanical testing and evaluation (2000) 802.
64. Y. Zhang , C.L. Hu, Z. Zhao, A.P. Li, X.L. Xu, W.B. Shi, Materials and Design 44 (2013) 612–621.
65. R. Branco, J.D. Costa, F.V. Antunes, Theoretical and Applied Fracture Mechanics 58 (2012) 28–34.
66. R. Zhu , X. Cai, Y. Wu, L. Liu, W. Ji, B. Hua, Materials and Design 53 (2014) 992–997.
67. M. Bayerlein, H.J. Christ, H. Mughrabi, Material Science and Engineering A 114 (1989) L11.

68. S.G.S. Raman, K.A. Padmanabhan, International Journal of Fatigue 17 (1995) 271.
69. T.S. Srivatsan, S. Anand, J.D. Troxell, International Journal of Fatigue 15 (1993) 355
70. M. Botshekan, S. Degallaix, Y. Desplanques, J. Polak, Fatigue Fracture Engineering and Material Structures 21 (1998) 651.
71. J.K. Mahato, P. Sarathi, A. Sarkar, A. Kundu, P.C. Chakraborthi, Procedia Materials Science 5 (2014) 1358–1367.
72. K. Dutta, K.K. Ray, Materials Science and Engineering A 540 (2012) 30–37.
73. A. Bhattacharyya, G. Subhash, N. Arakere, International Journal of Fatigue 59 (2014) 102–113.
74. A. Babaei, M.M. Mashhadi, Materials Characterization 101 (2015) 114–121.
75. C. Roy, V.V. Pavanan, G. Vishnu, P. Hari, M. Arivarasu, M. Manikandan, D.R. Kumar, N. Arivazhagan, Procedia materials science 5 (2014) 2503–2513.
76. M. Jafari, K. Tsuzaki, Journal of Alloys and Compounds 577S (2013) S636–S641.
77. T. Ungar, J. Gubicza, P. Hana, I. Alexandrov, Materials Science and Engineering A 319 – 321 (2001) 274–278.
78. T. Ungar, Materials Science and Engineering A, 309–310 (2001) 14–22.
79. G. Ribarik, T. Ungar, Materials Science and Engineering A 528 (2010) 112–121.
80. P.P. Seth, A. Das, H.N. Bar, S. Shivaprasad, A. Basu, K. Dutta, Journal of Materials Engineering and Performance 24 (2015) 2779–2783.
81. R. Kishore, L. Sahu, K. Dutta, A.K. Mondal, Materials Science and Engineering A 598 (2014) 299–303.

Bio Data

Name K. Divya Bharathi

Date of Birth 24.06.1992

Permanent Address H.No.:1-60/30/7,
Anjaiah Nagar,
Ranga Reddy, Hyderabad,
Telangana, India
Pin: 500084

E-mail ID k.divya.212@gmail.com

Languages Known English, Hindi, Telugu

Educational Qualifications:

Year	Degree/Certificate	Institution	Marks Obtained
2013	Bachelor of Technology (Metallurgical and Materials Engineering)	Mahatma Gandhi Institute of Technology	73% 1st Div.
2009	Intermediate	Narayana Junior College	85.6 1st Div.
2007	SSC	Z.P.H.S. Shakapoor	77.6 1st Div.

List of Publications:

1. K. Divya Bharathi, K. Dutta "Fatigue-Ratcheting Interaction Behavior of AISI 4340 steel" (Manuscript under preparation).
2. K. Divya Bharathi, K. Dutta "Stress ratio effect on ratcheting behavior of AISI 4340 steel" (Manuscript under preparation).